Dalton Transactions

Accepted Manuscript

ROYAL SOCIETY OF CHEMISTRY

www.rsc.org/dalton

We have amended the sentence as indicated by the referee to:
The magnetic susceptibility of CuNi(CN)4 has the value μ = 1.76 μB at 295 K, which is consistent with isolated moments on Cu2+ ions (d9), and unfortunately indicates that a delocalised electron system is not formed.

Journal Name

RSCPublishing

COMMUNICATION

Chemistry and Structure by Design: Ordered $CuNi(CN)_4$ Sheets with Copper(II) in a Square-Planar Environment

Cite this: DOI: 10.1039/xoxxoooooox

Received ooth January 2012,
Accepted ooth January 2012

DOI: 10.1039/xoxxoooooox

www.rsc.org/

A. M. Chippindale,*[a] S. J. Hibble,*[b] E. Marelli,[a] E. J. Bilbe,[a] A. C. Hannon[c] and M. Zbiri[d]

Journal Name

RSCPublishing

COMMUNICATION

Layered copper-nickel cyanide, $CuNi(CN)_4$, a 2-D negative thermal expansion material, is one of a series of copper(II)-containing cyanides derived from $Ni(CN)_2$. In $CuNi(CN)_4$, unlike in $Ni(CN)_2$, the cyanide groups are ordered generating square-planar $Ni(CN)_4$ and $Cu(NC)_4$ units. The adoption of square-planar geometry by Cu(II) in an extended solid is very unusual.

The simple binary copper(II) cyanide, $Cu(CN)_2$, does not exist. The reaction of Cu(II) in aqueous solution with the pseudohalide cyanide ion reacts via a number of steps to produce cyanogen and copper(I) cyanide, CuCN.[1] This is reminiscent of the reaction familiar to chemistry undergraduates in which the iodide ion reacts with copper(II) to produce iodine and copper(I) iodide.[2]

$$2Cu^{2+} + 4\,X^- = 2CuX + X_2 \quad (X = I^-, CN^-)$$

Our challenge was to stabilize Cu(II) with respect to the internal redox reaction in the presence of cyanide ligands only. This has been achieved by replacement of half of the Ni(II) in anhydrous nickel cyanide, $Ni(CN)_2$, by Cu(II) to form $CuNi(CN)_4$. In $Ni(CN)_2$, each Ni atom is linked by four linear, bridging cyanide ions to four other nickel atoms to form planar $Ni(CN)_2$ sheets with head-to-tail cyanide disorder.[3-5] By using the square-planar ion, $[Ni(CN)_4]^{2-}$, as a synthon and linking such units by Cu^{2+} ions, a modified $Ni(CN)_2$ sheet structure can be assembled in which the copper atoms have square-planar geometry and are coordinated only to cyanide ligands *via* nitrogen to generate an ordered sheet (Figure 1).[#]

Although there are a number of examples of molecular species containing square-planar Cu(II) with, for example, phthalocyanines and N and O donor ligands,[7,8] we believe that the layered product, $CuNi(CN)_4$, is the first example of a simple extended solid containing Cu^{2+} (d^9) ions in X-ray diffraction patterns of $CuNi(CN)_4$ at 30, 180 and 270 °C (303, 453 and 543 K) square-planar coordination. The separation between adjacent $CuNi(CN)_4$ layers at 3.09 Å is too great for significant interlayer interactions to occur, precluding Jahn-Teller distortion of octahedral geometry to produce (4+2) coordination, as is frequently observed in Cu^{2+} compounds. Further exploration of the Cu(II)-Ni(II) cyanide phase diagram shows that Cu(II) containing compounds also exist both as hydrates, $Cu_xNi_{1-x}(CN)_2{\cdot}3H_2O$, and dehydrated phases, $Cu_xNi_{1-x}(CN)_2$, forming solid solutions over the range ($0 \le x \le 0.25$).

The addition of Cu^{2+} ions to $Ni(CN)_4^{2-}$ in aqueous solution immediately produces a blue-green gelatinous precipitate (vide infra), which on stirring for several hours transforms to a grey solid, characterised as $CuNi(CN)_4$. On heating $CuNi(CN)_4$ under nitrogen at 680 K, copper(II) is reduced by cyanide to produce copper(I) cyanide and paracyanogen, together with nickel cyanide, according to the reaction:

$$Cu^{II}Ni(CN)_4 = Ni(CN)_2 + Cu^{I}CN + (CN)_n$$

Figure 2 shows the powder X-ray diffraction patterns obtained for $CuNi(CN)_4$ and $Ni(CN)_2$. The Bragg peak positions and relative intensities show the close underlying similarity of the two structures and confirm that $CuNi(CN)_4$ is a layered material. The difference in peak widths in the two diffraction patterns arises mainly from the difference in crystallite size of the two materials. The Raman spectrum of $CuNi(CN)_4$ exhibits 2 $\nu_{C\equiv N}$ stretches, at 2209 and 2184 cm^{-1}, and the infrared spectrum has one non-coincident $\nu_{C\equiv N}$ stretch at 2182 cm^{-1}. These observations are consistent with D_{4h} symmetry of the individual metal-cyanide layers. Only two arrangements of the

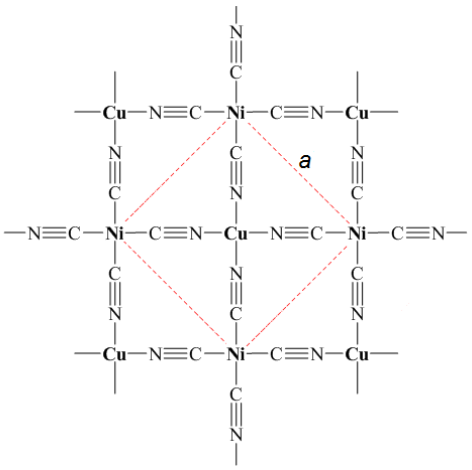

Fig. 1 Representation of a layer of $CuNi(CN)_4$ with square-planar geometry around both Cu^{2+} and Ni^{2+} ions. The structural repeat unit within the layer is shown in the red square of length *a*.

metal atoms and cyanide groups within each layer are therefore possible: namely, the one shown in Figure 1, with the carbon end of the cyanide ligand attached to nickel and the nitrogen end to copper, or the inverted arrangement with the carbon end attached to copper. Of these two possibilities, only the first arrangement yields a good fit to the low *r* region ($0 < r$ / Å < 3) of the total correlation function, $T^N(r)_{exp}$, obtained from neutron diffraction (Figure 3 and S.10) confirming that the metals and cyanide groups in $CuNi(CN)_4$ are indeed arranged as shown in Figure 1. The bond lengths obtained from the fitting of individual peaks in $T^N(r)_{exp}$ at 15 K are: C≡N, 1.1541(6); Ni–C, 1.857(1) and Cu–N, 1.943(2) Å.

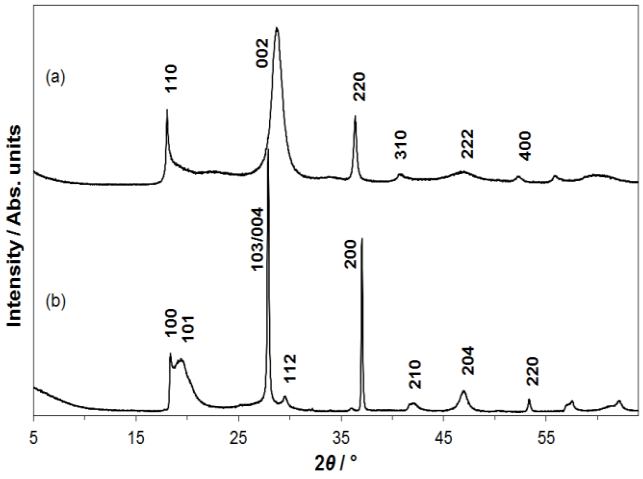

Fig. 2 Powder X-ray diffraction patterns at 295 K of (a) $CuNi(CN)_4$ (a = 6.957(1) and c = 6.180(6) Å) and (b) $Ni(CN)_2$ (a = 4.857 and c = 12.802 Å)[3] (Cu $K\alpha_1$ radiation, λ = 1.54060 Å) showing Miller indices of the principal reflections.

Taking into account the metal and cyanide ordering within the layers determined above, the powder X-ray diffraction pattern for

$CuNi(CN)_4$ can be indexed on a tetragonal unit cell (a = 6.957(1) and c = 6.180(6) Å) (Figure 2). This unit cell is related to that of $Ni(CN)_2$. The a lattice parameter in $CuNi(CN)_4$ is ~$\sqrt{2}$ of the value for $Ni(CN)_2$ as a consequence of the ordering of the Cu and Ni atoms within the layers. X-ray and neutron diffraction experiments[3] show no evidence of cyanide ordering within the nickel-cyanide layers in $Ni(CN)_2$ and in this case, the a lattice parameter corresponds to the direct M–CN–M distance shown in Figure 1. The c lattice parameter chosen for $CuNi(CN)_4$ corresponds to a two-layer repeat, *ABAB*, and a physically reasonable interlayer separation of ~3.09 Å. Although a c lattice parameter of 1/2 this value could be used to index fully the powder X-ray pattern of $CuNi(CN)_4$, this would be physically unreasonable as in the resulting *AAA* stacking, the atoms in adjacent layers would lie directly above each other and hence be impossibly close together. The stacking sequence in $Ni(CN)_2$ is more complicated with a four-layer repeat predominating[3,4] resulting in a c lattice parameter of ~12.8 Å and the appearance of the broad reflection, indexed as (101), seen at 2θ~20 ° (Figure 2(b)).

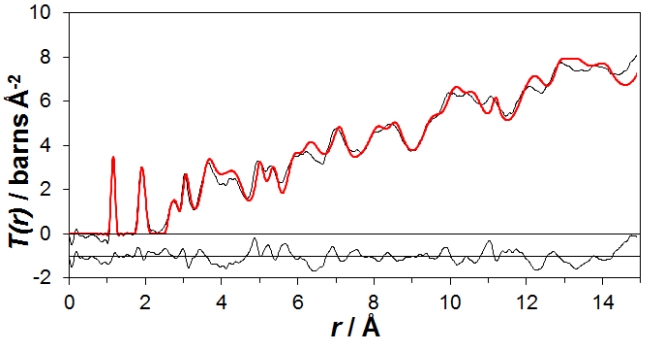

Fig. 3 Total correlation functions for $CuNi(CN)_4$ at 15 K: $T^N(r)_{exp,}$ (black line) and, for a model in *Cmcm*, $T^N(r)_{mod}$ (red line). The difference function is shown at the bottom of the plot (offset for clarity by 1 barns $Å^{-2}$).

Using the Cu–N, Ni–C and C≡N bond lengths obtained from fitting the low r region of $T^N(r)_{exp}$ (Figure 3), together with the unit-cell parameters obtained from the powder X-ray diffraction pattern and including the *ABAB* stacking of the layers, a 3-D model was constructed in space group *Cmcm* (Figure 4). This model reproduces $T^N(r)_{exp}$ to r = 15 Å well (Figure 3) and is thus a good representation of the short- and medium-range structure in the material.‡ It should be noted that this conventional crystallographic model does not fully reproduce the powder X-ray diffraction pattern in Figure 2 because in $CuNi(CN)_4$, there is extensive stacking disorder, as evidenced by the shape of the (110) reflection (Figure 2). Hence although the model gives a good description of the short- and medium-range order in $CuNi(CN)_4$, the chemically important information, it needs to be combined with a model of the stacking disorder in order to reproduce the powder X-ray pattern. Indeed, an appropriate calculation demonstrating this has already been carried out in a previous paper[4] in which different types of stacking disorder were considered for $Ni(CN)_2$ and has validity in the present case as the X-ray scattering factors of Cu and Ni are very similar (as indeed are those of C and N). The simulated powder X-ray diffraction pattern in which the sequence *AB* is followed by A occurs with a probability of 75% gives a good match to our observed pattern. In contrast, in $Ni(CN)_2$, the most probable stacking sequence (67%) is that the sequence *AB* is followed by a third layer, *A*', which is offset with respect to both *A* and *B*.

Layered inorganic materials are currently attracting much interest, particularly with respect to their electronic, optical and mechanical properties.[9] Although graphene and metal disulfides are the most widely studied, a recent paper utilising DFT calculations has suggested that $Ni(CN)_2$ should have interesting electronic properties when in the form of individual sheets and, by analogy with graphene, when rolled into nanotubes, particularly if it can be n or p doped.[10] Mo and Kaxiras proposed that doping could be achieved by replacing some of the –C≡N– linkages by –C≡C– or –N=N– groups to produce either p- or n- doped structures. In our synthesis of $CuNi(CN)_4$, we have effectively substituted on the metal sites in $Ni(CN)_2$, rather than the non-metal sites. By replacing half the Ni^{2+} by Cu^{2+} in $Ni(CN)_2$ to form $CuNi(CN)_4$, we have achieved an extremely high level of n doping of the layers. Measurement of the magnetic susceptibility of $CuNi(CN)_4$ shows paramagnetic behaviour over the temperature range 50-350 K, with μ = 1.76 μ_B at 295 K, which is consistent with isolated moments on Cu^{2+} ions (d^9), and unfortunately indicates that a delocalised electron system is not formed. The presence of an absorption band centred at ~17000 cm^{-1} in the diffuse reflectance spectrum of $CuNi(CN)_4$ can be ascribed to a *d-d* transition(s) and is unobserved in the corresponding spectrum of $Ni(CN)_2$ (Figure 5). From the reflectance spectra, the optical band gaps for $Ni(CN)_2$ and $CuNi(CN)_4$ are determined to be 16100 and 21780 cm^{-1} (2 and 2.7 eV), respectively, showing that this degree of substitution of Ni by Cu has produced a poorer semiconductor as a result of ordering within the metal-cyanide sheets.

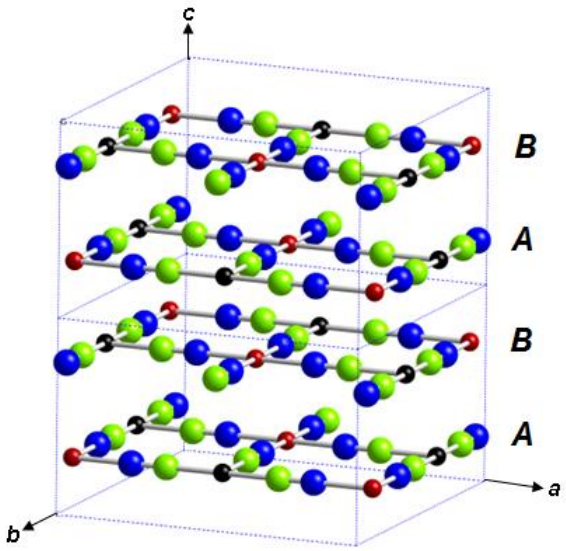

Fig. 4 Model of $CuNi(CN)_4$ in space group *Cmcm* (a = b = 9.9082 and c = 6.100 Å) showing the *ABAB* stacking of the ordered layers. (Key: copper atoms, orange spheres; nickel atoms, black spheres; carbon atoms, green spheres and nitrogen atoms, blue spheres).

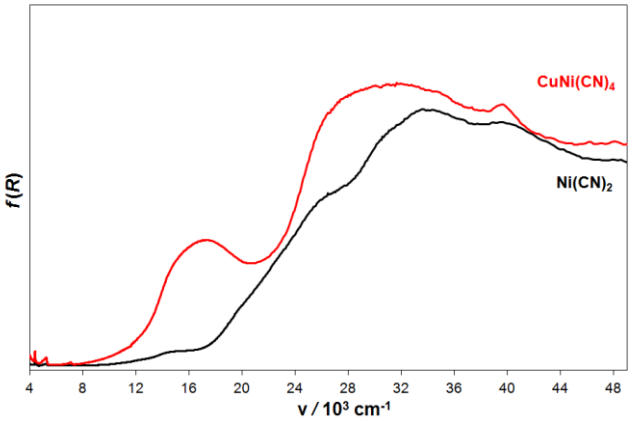

Fig. 5 Diffuse reflectance spectra of $CuNi(CN)_4$ (red) and $Ni(CN)_2$ (black)

Considering mechanical properties, $CuNi(CN)_4$ shows two-dimensional negative thermal expansion with $\alpha_a = -9.7(8) \times 10^{-6}$ K^{-1} (where $\alpha_a = (a_{T2} - a_{T1})/a_{T1}(T_2 - T_1)$ (Figure 6)) which is of a similar magnitude to that measured for graphene[11] and ~1.5 times the value for $Ni(CN)_2$. Inelastic neutron scattering and DFT studies on $Ni(CN)_2$ at ambient[5] and high pressure[12] show that it is the atomic motions perpendicular to the metal-cyanide sheets that give rise to the 2-D NTE behaviour and it is anticipated that similar mechanism will apply in the case of $CuNi(CN)_4$. Figure 6 shows the relative percentage changes in the *a* and *c* lattice parameters and cell volume, *V*, for $CuNi(CN)_4$ and $Ni(CN)_2$. Although α_a is independent of temperature over the temperature range of this study for both $CuNi(CN)_4$ and $Ni(CN)_2$, the temperature dependence of α_c is different for the two materials. For $CuNi(CN)_4$, α_c is non linear with temperature, whereas for $Ni(CN)_2$, it is, like α_a, independent of temperature. An explanation of the difference in the form of the variation of the *c* parameter with temperature, and hence also cell volume, requires a detailed comparison of the phonon density of states of $CuNi(CN)_4$ and $Ni(CN)_2$ to be carried out over a comparable temperature range.

As well as being mechanically different from $Ni(CN)_2$, copper nickel cyanide, $CuNi(CN)_4$, is chemically different in that it does not form hydrates. Indeed, it can be obtained directly from aqueous solution as the anhydrous compound, as described above. (Similar reactions using only nickel reagents, *e.g.* Ni^{2+} + $Ni(CN)_4^{2-}$, produce layered nickel-cyanide hydrates, $Ni(CN)_2.nH_2O$ (n = 3, 3/2), containing $Ni(NC)_4(H_2O)_2$ and $Ni(CN)_4$ units, and dehydration is required to form $Ni(CN)_2$).[3]

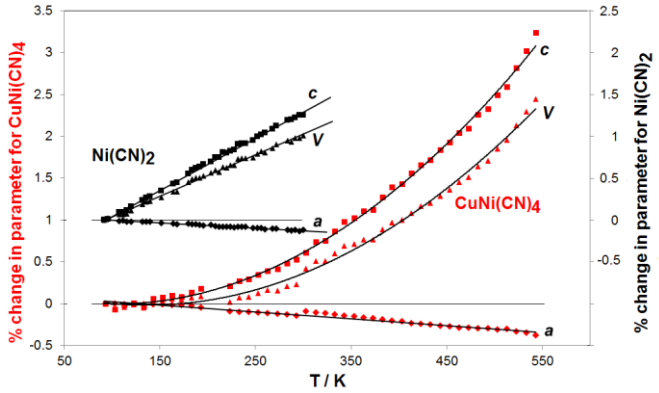

Fig. 6 The relative percentage changes in the *a* and *c* lattice parameters and volume, *V*, for $CuNi(CN)_4$ and $Ni(CN)_2$[3] over the temperature ranges (93 - 543) K and (95 - 295) K, respectively. The relative % change of a parameter, l_{T2}, is given by $100 \times (l_{T2} - l_{T1})/l_{T1}$, where l_{T2} is the parameter l at temperature T_2, and l_{T1} is the parameter l at the lowest temperature, T_1.

$CuNi(CN)_4$ is probably initially formed as individual layers. Mixing the salt solutions produces at first a blue gel, which turns grey on ageing in solution or on drying as the individual layers aggregate to form stacks. The powder X-ray diffraction patterns shown in Figure 7 provide evidence that the material grows only slowly in the [001] direction. Even in its final grey form, the stacks in $CuNi(CN)_4$ are only ~40 Å thick (as estimated by using the Scherrer equation applied to the (002) reflection). The slow growth in the *c* direction occurs possibly because the bonding between the layers is weak. Support for this hypothesis comes from the ease of separating the layers to make intercalation compounds. For example, stirring $CuNi(CN)_4$ in 4,4'-bipyridine in ethanol at room temperature produces a blue-grey solid with an interlayer separation of ~11.3Å, consistent with the formation of a pillared-layer compound, $CuNi(CN)_4(bipy)_x$, which is distinct from the previously reported material, $CuNi(CN)_4[bipy].(H_2O)_2$,[13] in which –$Cu(OH_2)_2$–NC–$Ni(CN)_2$–CN– zig-zag chains are linked through 4,4'-bipyridine groups.

Further exploration of the $Cu(CN)_2$-$Ni(CN)_2$ phase diagram required a different method of synthesis in which Cu^{2+} and Ni^{2+} were simultaneously added to a cyanide solution. Using this method at more nickel-rich compositions than $CuNi(CN)_4$ ($(Cu_{1/2}Ni_{1/2}(CN)_2$), mixtures of $CuNi(CN)_4$ and the hydrate $Cu_{1/4}Ni_{3/4}(CN)_2{\cdot}3H_2O$ were produced. At even higher nickel contents, a solid-solution region, $Cu_xNi_{1-x}(CN)_2{\cdot}3H_2O$ ($0 \le x \le 0.25$), formed. The hydrates can be easily dehydrated to form the $Cu_xNi_{1-x}(CN)_2$ phases shown in Figure 8, which all adopt a nickel-cyanide-type structure. No mixed Cu(II)-

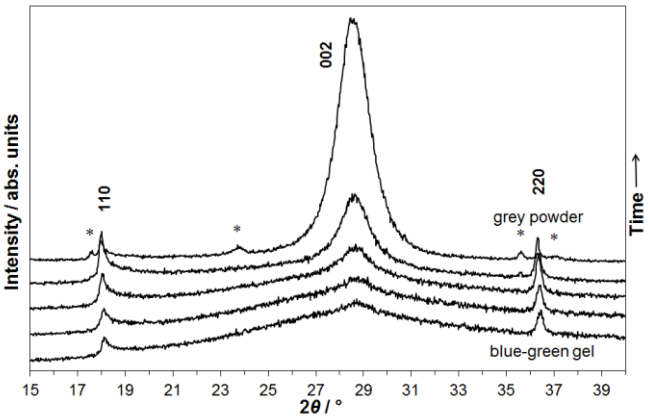

Fig. 7 *In situ* powder XRD patterns collected during the drying of $CuNi(CN)_4$ as the sample turned from a blue-green gelatinous solid to a grey powder. The (002) reflection at ~ 29 ° increases in intensity on drying, whilst the (110) and (220) reflections remain substantially unchanged as the number of already-formed 2-D layers stacking together increases.

Ni(II) cyanides containing more copper than nickel could be prepared and the additional copper Cu(II) is reduced to Cu(I) in the form of the low-temperature polymorph of copper (I) cyanide, LT-CuCN.[14] This reduction was also found when preparing the mixed Cu(I)-Cu(II) phase, $Cu_2Ni(CN)_5{\cdot}3H_2O$, from Cu(II) and $Ni(CN)_4^{2-}$.[15] In copper rich compounds, $Cu_xNi_{1-x}(CN)_2$ ($x > 0.5$), some Cu(II) atoms would have to be coordinated to the carbon end of cyanide groups and it might be this fact that leads to their instability. Although rare, it should be noted that Cu(II) can be attached to cyanide groups *via* the carbon end of the ligand, for example, in $[Cu(phen)_2CN]^+$,[16] and of particular note is the molecular compound, $Cu(phen)(CN)_2$, which has Cu(II) connected to two CN groups in this way.[17]

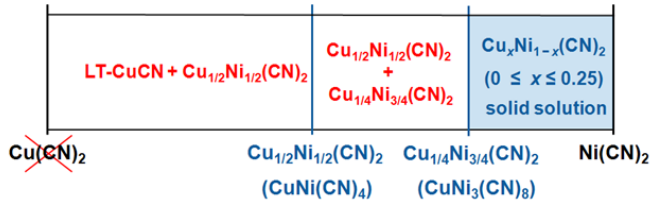

Fig. 8 Phases formed in the Cu(II)-Ni(II)-cyanide system.

In conclusion, we have prepared a number of new layered compounds, $Cu_xNi_{1-x}(CN)_2$, consisting of $M(CN)_2$ sheets structurally related to those found in $Ni(CN)_2$. Addition of the synthon, $[Ni(CN)_4]^{2-}$, to Cu^{2+} in aqueous solution, leads to the precipitation of anhydrous $CuNi(CN)_4$. A combination of powder X-ray and total neutron diffraction, together with vibrational spectroscopy, has established that in $CuNi(CN)_4$ ($(Cu_{1/2}Ni_{1/2}(CN)_2$), the cyanide ligands bind so that their carbon atoms are coordinated only to nickel

and their nitrogen atoms only to copper to generate ordered sheets containing square-planar $Ni(CN)_4$ and $Cu(NC)_4$ units. The stabilising of Cu^{II} in an environment with cyanide as the only ligand present has not previously been reported. $CuNi(CN)_4$ shows two-dimensional negative thermal expansion. We are currently analysing the phonon density of states of $CuNi(CN)_4$ to discover why it shows very different thermal expansion behaviour from $Ni(CN)_2$ perpendicular to the metal-cyanide layers.

In contrast to $CuNi(CN)_4$, which can be prepared directly as an anhydrous compound from aqueous solution, other, more nickel-rich $Cu_xNi_{1-x}(CN)_2$ compounds are formed *via* the hydrates, $Cu_xNi_{1-x}(CN)_2.3H_2O$, which can be easily dehydrated. A solubility gap exists between $CuNi(CN)_4$, the most copper-rich phase that can be formed and a region of solid solution which exists between $Cu_{1/4}Ni_{3/4}(CN)_2$ and $Ni(CN)_2$.

The authors thank the EPSRC (EP/G067279/1) and STFC (CMPC06101) for studentships for EM and EJB, respectively. The University of Reading is acknowledged for provision of the Chemical Analysis Facility (CAF).

Notes and references

[a] Department of Chemistry, University of Reading, Whiteknights, Reading RG6 6AD, UK. E mail: a.m.chippindale@rdg.ac.uk; Fax: +44 (0)1183786331; Tel: +44 (0)118 3788448

[b] present address: Jesus College, Oxford OX1 3DW, UK.

[c] ISIS Facility, Rutherford Appleton Laboratory, Chilton, Didcot, OX11 0QX, UK

[d] Institut Laue-Langevin, BP 156, F-38042 Grenoble Cedex 9, France

[#]FOOTNOTE: Although ordering of cyanide groups often occurs in mixed-metal cyanides, this is not always the case. For example, in the series of mixed-metal cyanides containing Cu(I), $(Cu_{1/2}Au_{1/2})CN$ contains ordered chains of the type $[Au{-}C{\equiv}N{-}Cu{-}N{\equiv}C{-}]_n$, whereas in $(Cu_{1/2}Ag_{1/2})CN$, there is head-to-tail cyanide disorder.[6]

[‡]FOOTNOTE: Although stacking together layers of D_{4h} symmetry in an *ABAB* sequence is incompatible with true tetragonal symmetry, it is possible to construct orthorhombic models with a tetragonal metric. Furthermore, stacking disorder will lead to the long-range average metric appearing tetragonal, so that a model describing the local and intermediate structure in *Cmcm* is not in conflict with the indexing of the powder X-ray pattern as tetragonal.

† Electronic Supplementary Information (ESI) available: Synthesis of $CuNi(CN)_4$ and $Cu_xNi_{1-x}(CN)_2$ phases; X-ray powder diffraction patterns (variable temperature); neutron powder total diffraction details; thermal analysis; IR and Raman spectroscopy data, magnetic data. See DOI: 10.1039/c000000x/

1 A. G. Sharpe in 'The Chemistry of Cyano Complexes of the Transition Metals', Academic Press Inc London, 1976.
2 C. E. Housecroft and A. G. Sharpe, Inorganic Chemistry, Pearson Education Ltd, UK, 4th Edn, p 768.
3 S. J. Hibble, A. M. Chippindale, A. H. Pohl and A. C. Hannon, *Angew. Chem. Int. Ed.*, 2007, **46**, 7116.
4 A. L. Goodwin, M. T. Dove, A. M. Chippindale, S. J. Hibble, A. H. Pohl and A. C. Hannon, *Phys. Rev B: Condens. Matter.*, 2009, **B80**, 054101.
5 R. Mittal, M. Zbiri, H. Schober, E. Marelli, S. J. Hibble, A. M. Chippindale and S. L. Chaplot, *Phys. Rev B: Condens. Matter.*, 2011, **B83**, 024301.
6 A. M. Chippindale, S. J. Hibble, E. J. Bilbé, E. Marelli, A. C. Hannon, C. Allain, R. Pansu, and F. Hartl, *J. Am .Chem..Soc.*, 2012, **134**, 16387.
7 C. J. Brown, *J. Chem. Soc. A*, 1968, 2488.
8 M. Melnik, M. Kabesova, M. Dunaj-Jurco and C. E. Holloway, *J. Coord. Chem.*, 1997, **41**, 35.
9 Q. H. Wang, K. Kalantar-Zadeh, A. Kis, J. N. Coleman and M. S. Strano, *Nature Nanotechnol*, 2012, **7**, 699.
10 Y. Mo and E. Kaxiras, *Small*, 2007, **3**, 1253.
11 D. Yoon, Y. W. Son and H. Cheong *Nano Lett.*, 2011, *11*, 3227.
12 S. K. Mishra, R. Mittal, M. Zbiri, R. Rao, P. Goel, S. J. Hibble, A. M. Chippindale, T. Hansen, H. Schober and S. L. Chaplot, arXiv:1409.2305 [cond-mat.mtrl-sci].
13 O. Sereda and H. Stoeckli-Evans, *Acta Cryst.*, 2008, **C64**, m221.
14 S. J. Hibble, S. G. Eversfield, A. R. Cowley and A. M. Chippindale, *Angew. Chem. Int. Ed.* **2004**, *43*, 628.
15 Y. L. Qin, R. X. Yao, G. X. Wu, M. M. Liu, and X. M. Zhang, *Chem. Asian J.*, 2013, **8**, 1587.
16 M. Dunaj-Jurco, I. Potocnak, J. Cibik and M. Kabesova, V. Kettmann And D Miklos, *Acta Cryst.* 1993, **C49**, 1479.
17 M. Wicholas and T. Wolford, *Inorg. Chem.*, 1974. **13**, 316.

Graphical Abstract

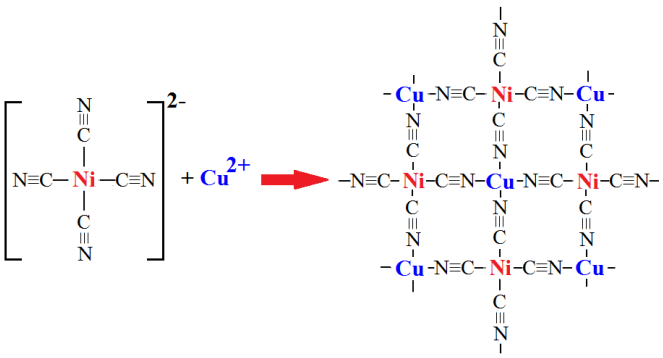

Cu(II) has been stabilised with square-planar coordination in a cyanide-only environment in the layered semiconducting material, copper-nickel cyanide, $CuNi(CN)_4$, which shows 2-D negative thermal expansion.

Supporting Information for Publication

Chemistry and Structure by Design: Ordered $CuNi(CN)_4$ Sheets with Copper(II) in a Square-Planar Environment

Ann M. Chippindale,*[,a] Simon J. Hibble,*[,b] Edward J. Bilbé,[a] Elena Marelli,[a]

Alex C. Hannon[c] and Mohamed Zbiri

[a] Department of Chemistry, University of Reading, Whiteknights, Reading RG6 6AD, U.K.

[b] Present address: Jesus College, Oxford OX1 3DW, UK

[c] ISIS Facility, Rutherford Appleton Laboratory, Chilton, Didcot OX11 0QX, U.K.

[d] Institut Laue-Langevin, BP 156, F-38042 Grenoble Cedex 9, France

EMAIL ADDRESSES FOR CORRESPONDENCE:

a.m.chippindale@rdg.ac.uk; simon.hibble@rdg.ac.uk

1. Synthesis and Characterisation of Mixed Copper(II)-Nickel(II) Cyanide, $CuNi(CN)_4$

1.1 Synthesis of $CuNi(CN)_4$

Caution! Soluble cyanide compounds can be extremely toxic if inhaled, swallowed or absorbed through the skin. They should be handled with care wearing gloves and safety glasses in a ventilated area, especially when preparing samples of gram quantities needed for neutron diffraction.

$K_2Ni(CN)_4 \cdot nH_2O$ (Aldrich) (5.3020 g, ~0.0220 mol) was dissolved in distilled water (110 ml) and added to an aqueous solution (110 ml) of $CuSO_4 \cdot 5H_2O$ (Aldrich) (5.4899 g, 0.0296 mol) at room temperature. A blue-green gelatinous solid formed immediately. This was stirred for four hours during which time, it turned grey in colour. It was then filtered, repeatedly washed with distilled water and allowed to dry in air. The dry product was in the form of a fine grey powder. The Cu:Ni ratio of 1:1 was confirmed by the total neutron diffraction analysis (Section 2, page S10) and the absence of water by IR and Raman spectroscopy (Section 1.2, page S4) and thermogravimetric analysis (Section 1.4, page S7). Atomic Absorption analysis: Cu:Ni 0.98:1.00. Combustion analysis: Found C: 20.79; N: 23.71; H: < 0.10 % [Calc. for $CuNi(CN)_4$ C: 21.23; N: 24.76; H: 0; Cu: 28.08; Ni 25.93 %]. The powder X-ray diffraction patterns at room temperature and over a range of temperatures are given in Sections 1.3 and 3.2 (pages S6 and S18, respectively).

1.2 IR and Raman Spectra of $CuNi(CN)_4$

Infrared and Raman spectra were measured at room temperature on undiluted powder samples using a Perkin Elmer spectrum 100 FT-IR spectrometer with a Universal Attenuated Total Reflection sampling accessory and a Renishaw InVia Raman microscope (λ_{exc} = 633 nm), respectively (Figures S.1 and S.2).

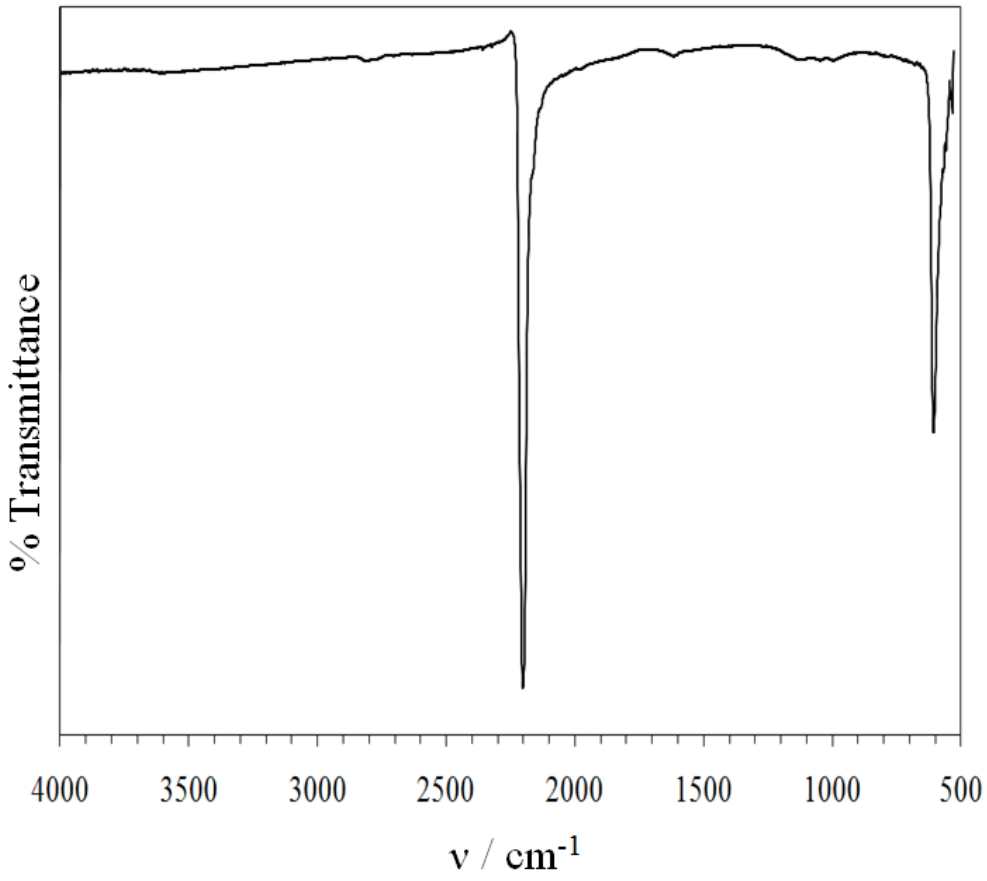

Figure S.1: IR spectrum of grey polycrystalline $CuNi(CN)_4$

(ν(C≡N) 2181(s, broad); ν(Cu–N, Ni–C) 576(w) cm^{-1}).

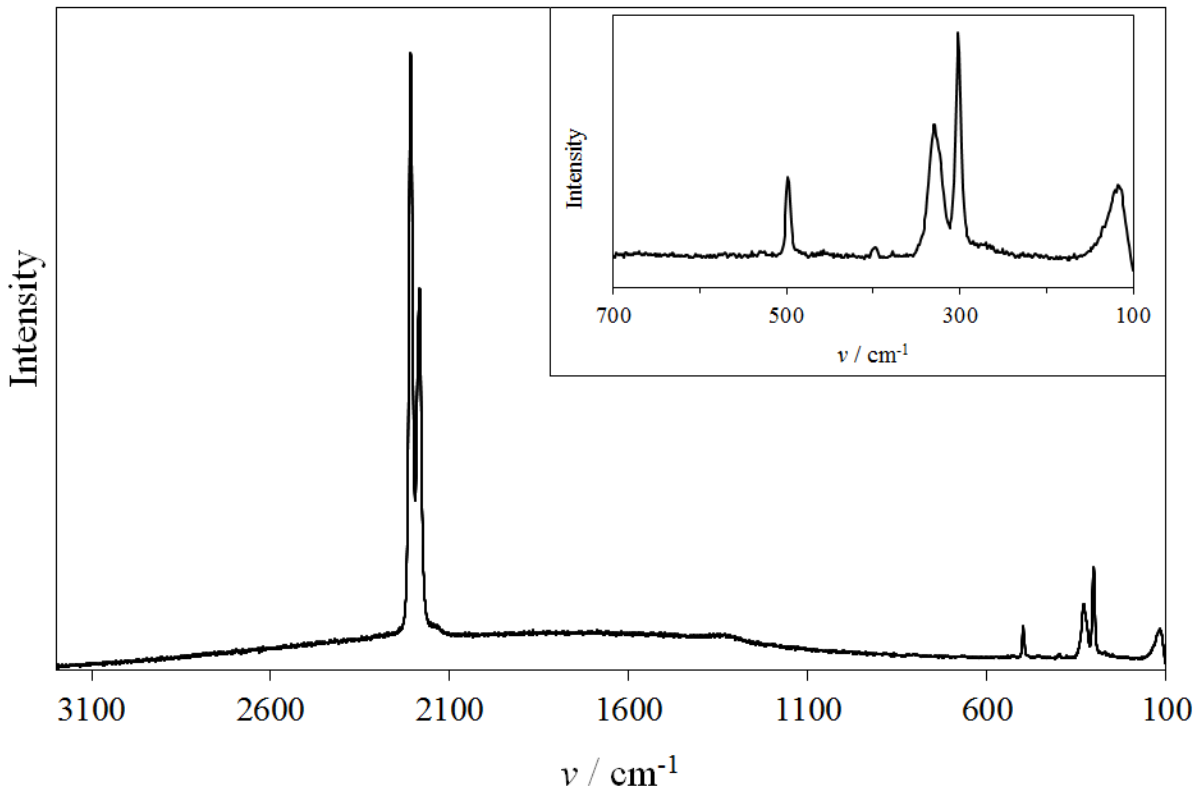

Figure S.2: Raman spectrum of grey polycrystalline $CuNi(CN)_4$

(ν(C≡N) 2209(s), 2184(s); ν(Cu–N, Ni–C) 498 (vw); low frequency bends: 398 (vvw, broad), 329(vw, broad), 301(w), 123(vw, broad) cm^{-1}).

1.3 Room-temperature Powder X-ray Diffraction

Room-temperature powder X-ray diffraction data were measured using a Bruker D8 diffractometer (Cu Kα1 radiation, λ = 1.54060 Å) operating in Bragg-Brentano geometry using standard poly(methyl methacrylate) sample holders (Figure S.3).

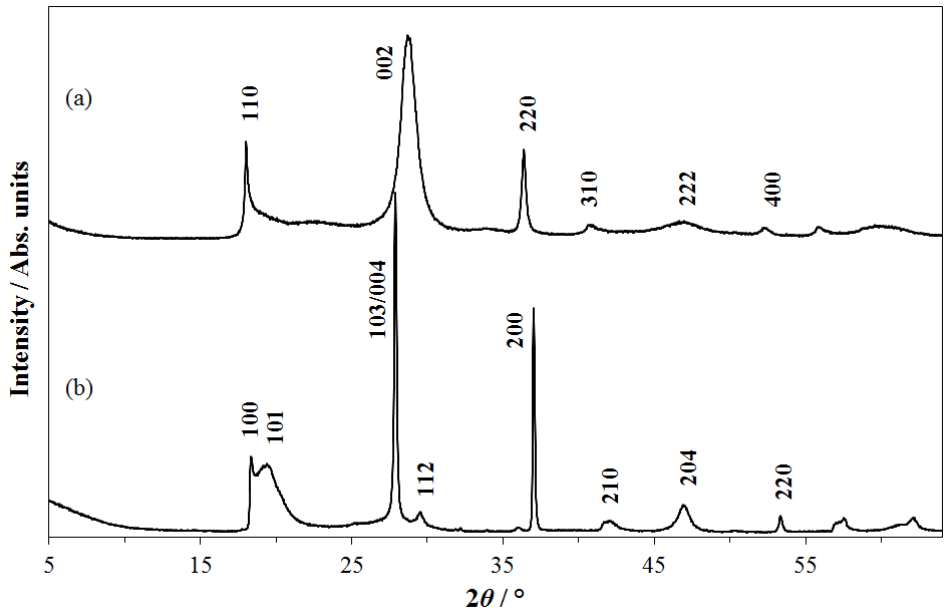

Figure S.3: Powder X-ray diffraction patterns at 295 K of (a) $CuNi(CN)_4$ (a = 6.957(1) and c = 6.180(6) Å) and (b) $Ni(CN)_2$ (a = 4.857 and c = 12.802 Å) (Cu Kα1 radiation, λ = 1.54060 Å)[1].

1.4 Thermal Analysis of $CuNi(CN)_4$

Thermal analyses of $CuNi(CN)_4$, was performed under dry N_2 between 288 and 680 K at a heating rate of 1 K min^{-1} using a TA Q600 STD, simultaneous TGA/DSC instrument (Figure S.4).

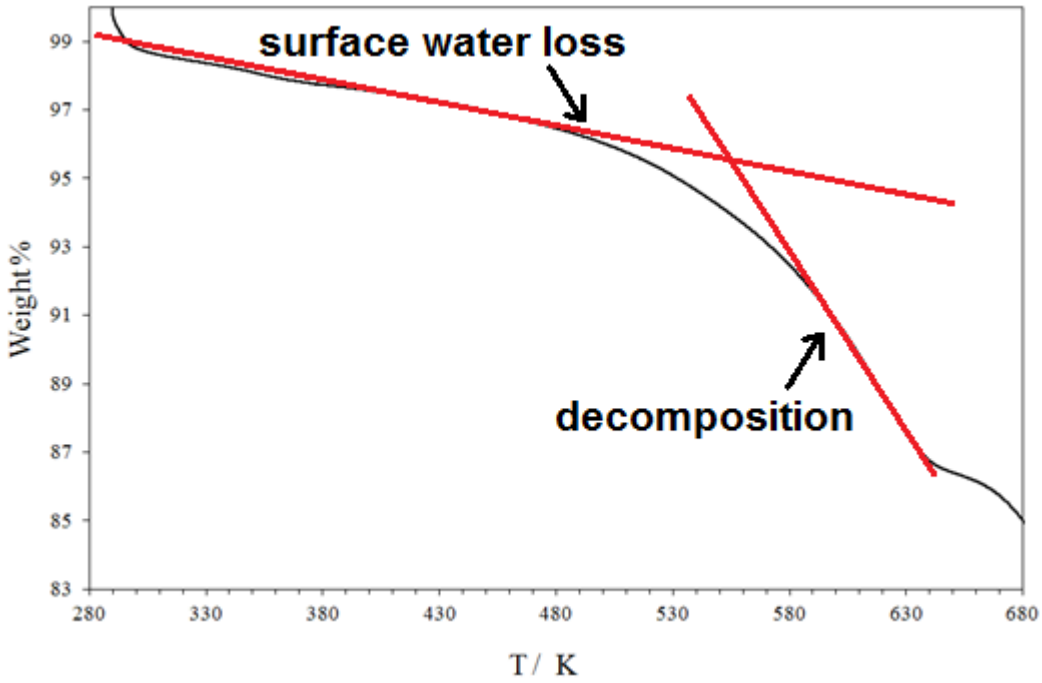

Figure S.4: TGA over the range 288-680 K for $CuNi(CN)_4$. The initial weight loss is due to surface water followed by decomposition from ~565 K.

The IR spectrum of the dark-brown product (Figure S.5), shows peaks at 2200(s) and 2169(s) cm^{-1}, which agree well with the literature values of 2199 and 2170 cm^{-1} for ν(C≡N) for $Ni(CN)_2$[1] and HT–CuCN[2] respectively. The broad peak at 1350 cm^{-1} is assigned to ν(C=N) of paracyanogen, $(C=N)_n$,[3] the polymeric form of cyanogen, $(CN)_2$, which has been observed previously as a product on heating mercuric cyanides.[4, 5] The formation of paracyanogen also explains the dark colour of the heated product. The powder X-ray diffraction pattern of the final product clearly contains peaks from $Ni(CN)_2$[1] and HT–CuCN[2] (Figure S.6) (N.B paracyanogen, a disordered polymer, has no observable peaks in the diffraction pattern).

Thus at 635 K under N_2, the overall reaction is: $Cu^{II}Ni(CN)_4 = Ni(CN)_2 + Cu^{I}CN + (CN)_n$

The loss of one cyano group as ½$(CN)_2$ from $CuNi(CN)_4$ has a calculated weight loss = 11.50%.

S8

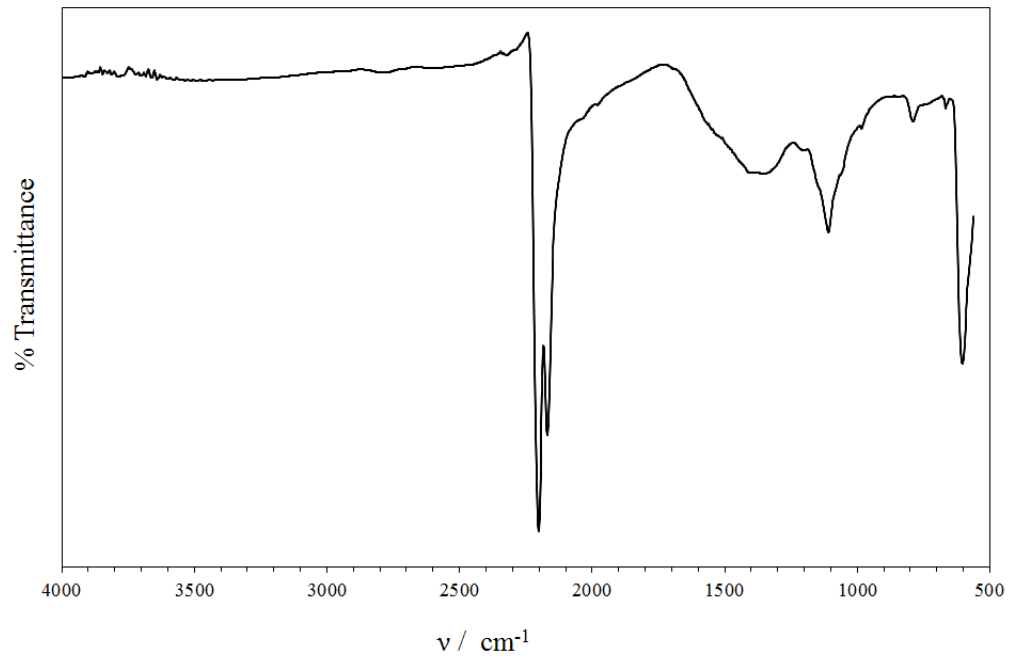

Figure S.5: IR spectrum of the product formed after heating $CuNi(CN)_4$ under N_2 in thermogravimetric balance The peaks at 2200(s) and 2169(s) cm^{-1}, agree well with the literature values for ν(C≡N) for $Ni(CN)_2$[1] and HT–CuCN.[2]

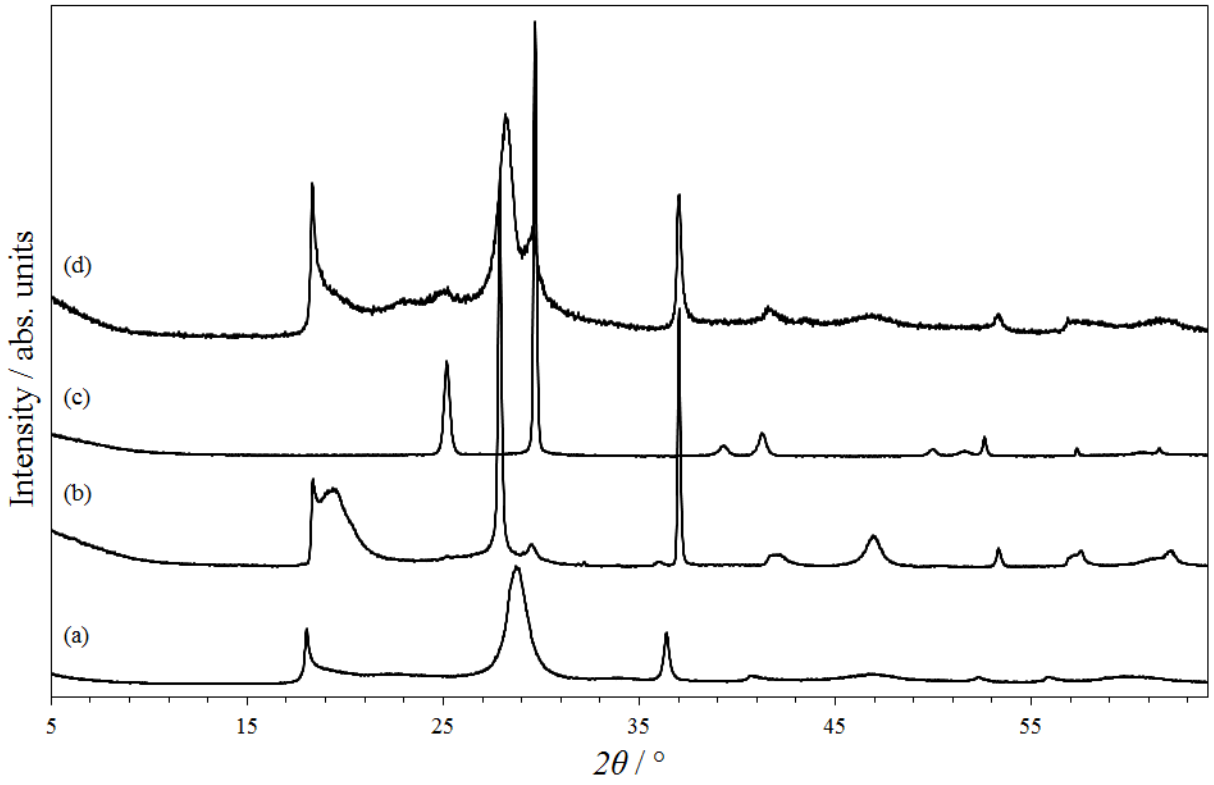

Figure S.6: Powder X-ray diffraction patterns of (a) $CuNi(CN)_4$, (b) $Ni(CN)_2$, (c) HT–CuCN and (d) the product on heating $CuNi(CN)_4$ to 680 K under N_2.

1.5 Magnetic and Diffuse Reflectance Measurements

The magnetic moment of $CuNi(CN)_4$ was measured over the range ($1.83 \leq T$ / K ≤ 350) using a SQUID magnetometer by Dr R. K. Kremer, Max-Planck Institut für Festköperforschung, Stuttgart (Figure S.7).

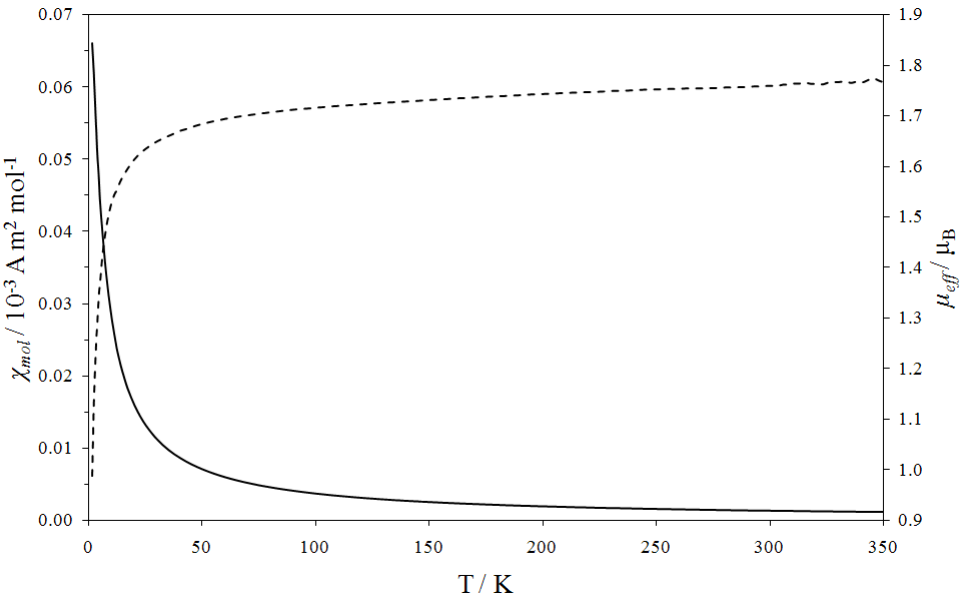

Figure S.7: Molar magnetic susceptibility, χ_{mol} (solid line), and effective magnetic moment, μ_{eff} (dashed line) measured for $CuNi(CN)_4$ over the temperature range 1.83-350 K.

The effective magnetic moment, μ_{eff}, at 295 K is 1.76 μ_B.

Diffuse reflectance spectra were collected for $CuNi(CN)_4$ and $Ni(CN)_2$ over the range 4000 – 49000 cm^{-1} on a Perkin Elmer 900 UV-Vis-NIR spectrometer equipped with a 60 mm diameter integrating sphere (Figure 5). The polycrystalline samples were loaded into a black sample holder with a 1 cm quartz window and the reflectance spectrum measured in the form of the Kubelka-Munk function, $f(R)$.[6]

$$f(R) = \frac{(1-R)^2}{2R} = \frac{k}{s} = \frac{Ac}{s}$$

where R is the reflectance, k the absorption coefficient, s the scattering coefficient, A the absorbance and c the concentration of the absorbing species.

2. Neutron Diffraction and Density Studies of $CuNi(CN)_4$

2.1 Pyknometric Density Measurement

The density of $CuNi(CN)_4$ was measured at room temperature using a Quantachrome Micropycnometer with helium gas as the working fluid. The density obtained was 2.439 g cm^{-3} in excellent agreement with the crystallographic density of 2.440 g cm^{-3} calculated using the unit-cell parameters determined at 295 K (Figure 2) and unit-cell content, Z, equal to 2.

2.2 Neutron Diffraction Studies of $CuNi(CN)_4$

The sample of $CuNi(CN)_4$ (1.7665 g) used in the neutron diffraction experiments was dried at 110 °C under N_2 for 4 hours prior to loading into a 6mm diameter, thin-walled vanadium can under an argon atmosphere.

Time-of-flight total neutron diffraction data were collected on the GEM diffractometer[7,8] at the ISIS facility, Rutherford Appleton Laboratory, Chilton, UK. The vanadium can containing the sample was placed in the instrument sample tank inside a close-circuit refrigerator (CCR). Data were collected at both 15 and 295 K using this experimental setup. The packing densities used in the data correction process were determined from the weight of the samples and can dimensions. Background runs to correct the data were collected on the empty instrument, empty can and on a standard vanadium rod. The data from detector banks 2, 3, 4 and 5 at mean scattering angles 17.3, 34.3, 61.7 and 91.8° were corrected for multiple and backscattering, attenuation and inelasticity and normalized to absolute scattering cross-section units using the program GudrunGUI[9] and the magnetic self scattering derived from the Cu^{2+} (d^9) atoms was subtracted to obtain the final distinct scattering. The corrected data were merged to yield an interference function, $Qi^N(Q)$, over the Q range 0.7 – 49 $Å^{-1}$ using the suite of programs ATLAS[10] in OpenGenie.[11] The low r region was extrapolated to Q = 0 $Å^{-1}$ using a quadratic function applied to the data between 0.7 and 1 $Å^{-1}$ (Figure S.8).

The interference function was then multiplied by the Lorch modification function[12] before the total correlation function, $T^N(r)_{exp,}$ was obtained *via* Fourier transformation (Figure S.9). Use of the Lorch function eliminates termination ripples in $T^N(r)_{exp}$. The total correlation function, $T^N(r)_{exp}$, obtained in this manner was used in the modelling studies (Section 2.3). N.B. The coherent scattering lengths, $\bar{b}$, for used for Cu, Ni, C and N were 7.718, 10.3, 6.646 and 9.36 fm respectively.[13]

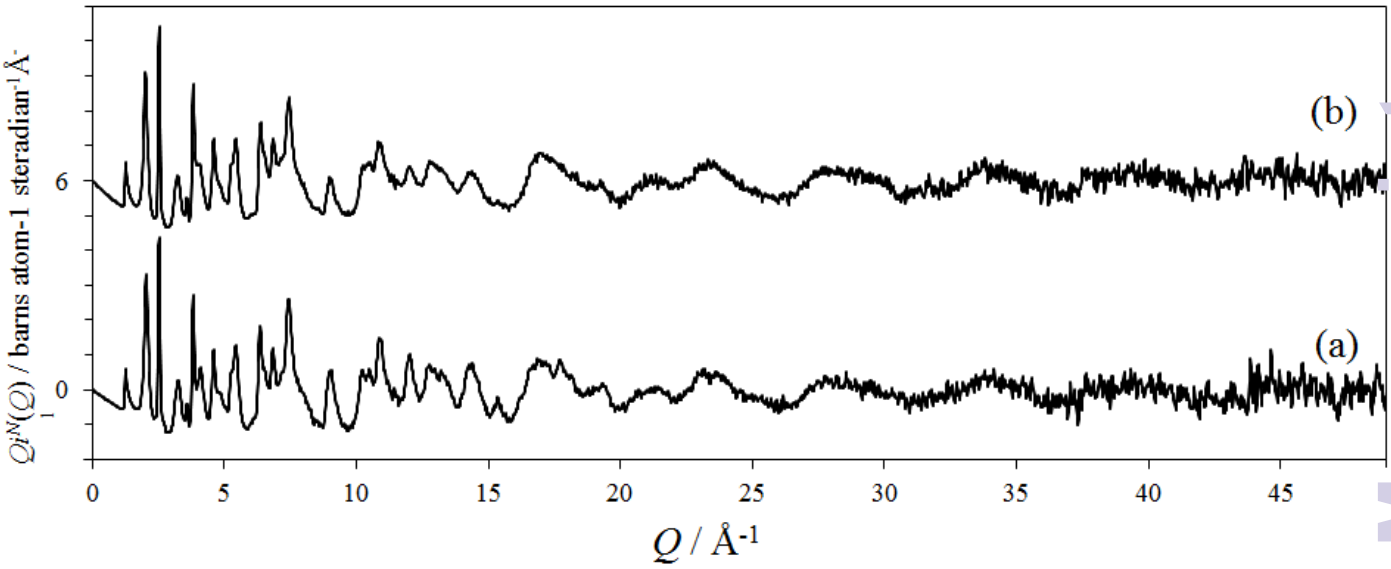

Figure S.8: The interference function, $Qi(Q)$, for $CuNi(CN)_4$ from neutron scattering at (a) 15 K and (b) 295 K (offset for clarity by 6 barns atom^{-1} steradian^{-1}Å^{-1}).

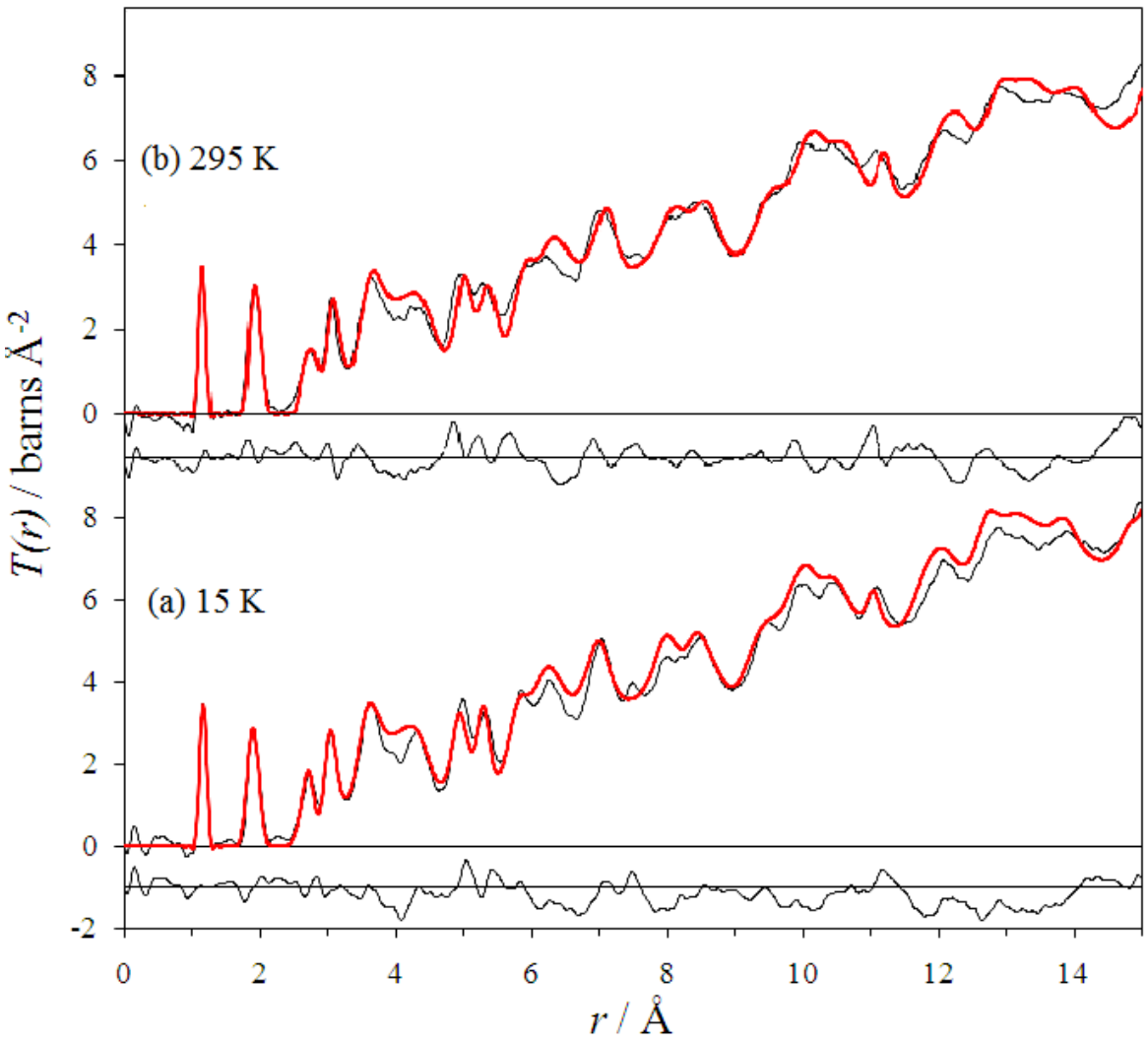

Figure S.9: Total correlation functions, $T^N(r)_{exp,}$ (black line) and $T^N(r)_{mod}$ (red line) for the model in *C mcm*, for $CuNi(CN)_4$ at (a) 15 K and (b) 295 K. The difference function is shown at the bottom of each plot (offset for clarity by 1 barns Å^{-2}).

Figure S.10 shows low-r region of the $T^{N}(r)$ correlation function calculated without using the Lorch function. The advantage of this unmodified transformation is that it is easier to see, particularly in the region $2.5 \leq r$ / Å ≤ 3, that the cyanide linkages must be arranged in the sense Ni–C≡N–Cu in $CuNi(CN)_4$. However this figure does show large termination ripples that can lead to confusion in identifying peaks. Hence the data shown in Figure S.9 was used for structural modelling.

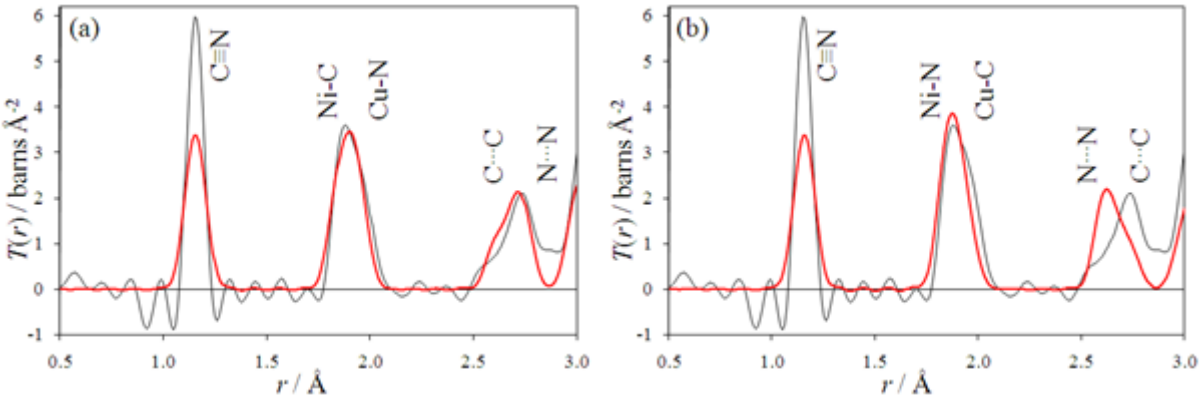

Figure S.10: The low-r region of the $T^{N}(r)$ correlation function of $CuNi(CN)_4$ at 15 K calculated using the step function (thin black line). The $T^{N}(r)_{mod}$ (red line) correlation functions are calculated with a broadening factor of 0.05 Å for every correlation (clearly far from ideal for the C≡N correlation). In (a), the model consists of $Ni(CN)_4$ and $Cu(NC)_4$ units linked through Ni–C≡N–Cu bridges and in (b) $Ni(NC)_4$ and $Cu(CN)_4$ units are linked through Ni–N≡C–Cu bridges. Model (a) gives the best fit, particularly at ($2.5 \leq r$ / Å ≤ 3), supporting the proposal that Ni is bonded to C and Cu to N within the layers of $CuNi(CN)_4$.

Table S.1: Fitted peaks positions, *r*, for $CuNi(CN)_4$ at 15 and 295 K from $T^N(r)_{exp}$ (Figure S.9)

	Atomic pair	*r* / Å	
		15 K	295 K
	C≡N	1.1541(6)	1.1541(6)
	Ni–C	1.857(1)	1.859(2)
	Cu–N	1.943(2)	1.947(2)
*a**/ Å[i]		7.006(2)	7.015(3)
a / Å[ii]			6.957(1)

[i] Values calculated as $a^* = \sqrt{2}\,(d_{Cu–N} + d_{C\equiv N} + d_{Ni–C})$ using the sheet model shown in Figure 1

[ii] Value from PXRD pattern at 295 K (Figure 2)

2.3 Modelling $T^N(r)_{exp}$

Using the Cu–N, Ni–C and C≡N distances determined from $T^N(r)_{exp}$ (Table S.1), it is possible to calculate the length of the side of the square structural repeat unit for one layer of $CuNi(CN)_4$, as shown in Figure 1. At 295 K, this length, *a**, is slightly longer than the value, *a*, obtained from powder X-ray diffraction. This discrepancy arises because in calculating *a**, no account is taken of the lateral thermal displacements of the atoms (see ref [14] for further discussion and justification of the use of *a** for modelling of $T^N(r)$ data).

In order to produce a three-dimensional model of the structure of $CuNi(CN)_4$ incorporating the stacking of the layers, it is necessary to chose a larger structural repeat unit within the layer *i.e.* $\sqrt{2} \times a^*$. In this way, a structural model can be constructed in space group *Cmcm* which fits both the short- and medium-range order as indicated by the good fit to $T^N(r)_{exp}$ (Figure S.9). It should be noted that although the space group is

orthorhombic, we use a tetragonal metric. Overall stacking disorder will lead to pseudotetragonal symmetry, even though this is untrue on a local scale.

Table S.2: Fractional atomic coordinates for $CuNi(CN)_4$ at 15 K used to construct the $T^N(r)_{mod}$ in *Cmcm* with $a = b =$ 9.9082 and $c = 6.100$ Å. N.B. all sites are fully occupied

Atom	Site	*x*	*y*	*z*
Ni	4*c*	0	0.6250	1/4
Cu	4*c*	0	0.1250	1/4
C(1)	4*c*	0	0.8124	1/4
N(1)	4*c*	0	0.9289	1/4
C(2)	4*c*	0	0.4376	1/4
N(2)	4*c*	0	0.3211	1/4
C(3)	8*g*	0.1874	0.6250	1/4
N(3)	8*g*	0.1961	0.1250	1/4

R-factor[15], $R_{T(r)} = 6.92$ % ($0 < r \leq 15$) and 6.45 % ($5 \leq r \leq 15$)

where $R_{T(r)} = \left(\sum_i \left(T^N(r_i)_{exp} - T^N(r_i)_{model} \right)^2 \Big/ \sum_i \left(T^N(r_i)_{exp} \right)^2 \right)^{½}$

Table S.3: Root-mean-square, $\langle u^2 \rangle^{1/2}$, values (Å) used to broaden the individual partial correlation functions to calculate the $T^{N}(r)_{mod}$ for $CuNi(CN)_4$ at 15 K.

Atom pairs	Intra-layer correlations		
Ni•••Ni Cu•••Cu	$r \leq 15.0$ Å $\langle u^2 \rangle^{\frac{1}{2}} = 0.1$		
Cu•••Ni	$r \leq 15.0$ Å $\langle u^2 \rangle^{\frac{1}{2}} = 0.07$		
Ni–C Cu–N	$r \leq 3.0$ Å $\langle u^2 \rangle^{\frac{1}{2}} = 0.058$	$3.0 < r \leq 5.0$ Å $\langle u^2 \rangle^{\frac{1}{2}} = 0.08$	$5.0 < r \leq 15.0$ Å $\langle u^2 \rangle^{\frac{1}{2}} = 0.12$
Ni•••N Cu•••C	$r \leq 4.0$ Å $\langle u^2 \rangle^{\frac{1}{2}} = 0.058$	$4.0 < r \leq 6.0$ Å $\langle u^2 \rangle^{\frac{1}{2}} = 0.08$	$6.0 < r \leq 15.0$ Å $\langle u^2 \rangle^{\frac{1}{2}} = 0.18$
C≡N	$r \leq 3.0$ Å $\langle u^2 \rangle^{\frac{1}{2}} = 0.027$	$3.0 < r \leq 6.0$ Å $\langle u^2 \rangle^{\frac{1}{2}} = 0.12$	$6.0 < r \leq 15.0$ Å $\langle u^2 \rangle^{\frac{1}{2}} = 0.18$
C•••C	$r \leq 3.0$ Å $\langle u^2 \rangle^{\frac{1}{2}} = 0.078$	$3.0 < r \leq 15.0$ Å $\langle u^2 \rangle^{\frac{1}{2}} = 0.18$	
N•••N	$r \leq 3.0$ Å $\langle u^2 \rangle^{\frac{1}{2}} = 0.063$	$3.0 < r \leq 15.0$ Å $\langle u^2 \rangle^{\frac{1}{2}} = 0.18$	

Table S.3 (continued)

Atom pairs	Inter-layer correlations		
Ni•••Ni Cu•••Cu Ni•••Cu	$r \leq 7.0$ Å $\langle u^2 \rangle^{\frac{1}{2}} = 0.25$	$7.0 < r \leq 15.0$ Å $\langle u^2 \rangle^{\frac{1}{2}} = 0.3$	
Cu•••N Ni•••C Cu•••C Ni•••N	$r \leq 4.0$ Å $\langle u^2 \rangle^{\frac{1}{2}} = 0.18$	$4.0 < r \leq 7.0$ Å $\langle u^2 \rangle^{\frac{1}{2}} = 0.25$	$7.0 < r \leq 15.0$ Å $\langle u^2 \rangle^{\frac{1}{2}} = 0.35$
N•••C N•••N C•••C	$r \leq 5.5$ Å $\langle u^2 \rangle^{\frac{1}{2}} = 0.2$	$5.5 < r \leq 9.0$ Å $\langle u^2 \rangle^{\frac{1}{2}} = 0.22$	$9.0 < r \leq 15.0$ Å $\langle u^2 \rangle^{\frac{1}{2}} = 0.4$

3. Negative Thermal Expansion Studies of $CuNi(CN)_4$

3.1 Variable-temperature Powder Neutron Diffraction Studies

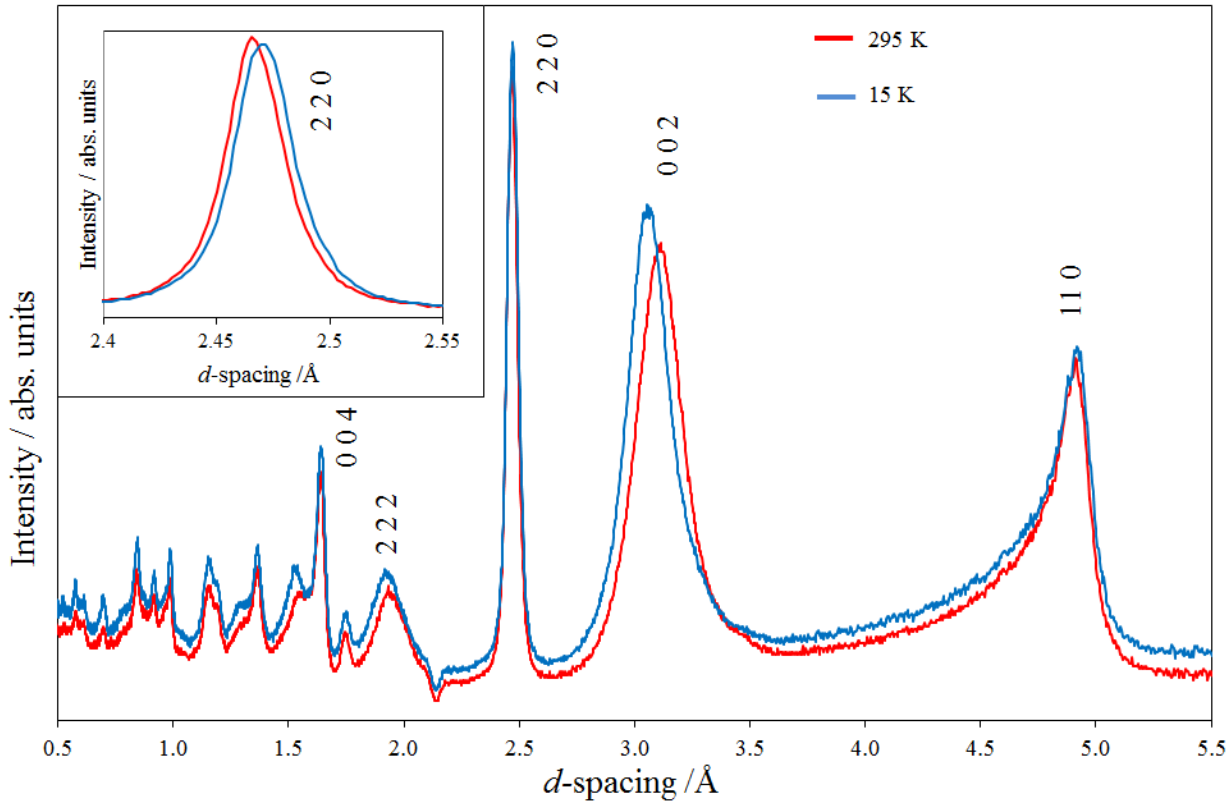

Figure S.11: Powder neutron diffraction pattern of $CuNi(CN)_4$ at 15 K (blue) and 295 K (red) showing the positive thermal expansion along the *c* direction (peak at ~3 Å) and the negative thermal expansion in the *ab* plane (peak at ~4.75 Å) (see inset).

3.2 Variable-temperature Powder X-ray Diffraction Studies

In situ variable-temperature X-ray studies, to investigate the thermal expansion behavior of $CuNi(CN)_4$, were performed using an Anton Parr TTK 450 sample chamber operating under vacuum over the temperature range 93-603 K attached to a Bruker D8 diffractometer (Cu $K\alpha_1$ radiation, λ = 1.54060 Å) (See Figure 6 and Table S.4). $CuNi(CN)_4$ is stable up to 543 K (Figures S.12 and S.13) consistent with the TGA results (Section S.4)

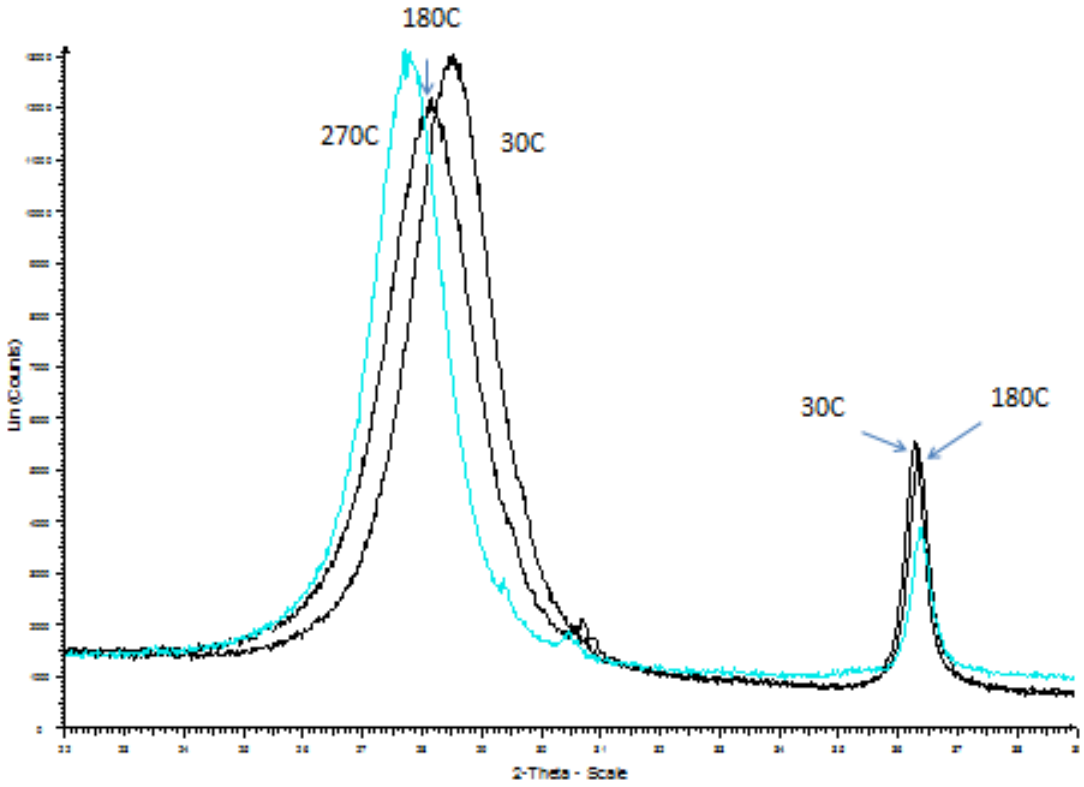

Figure S.12: Powder X-ray diffraction patterns of $CuNi(CN)_4$ at 30, 180 and 270 °C (303, 453 and 543 K) showing the positive thermal expansion along the *c* direction ((002) peak at 2θ ~28 °) and the negative thermal expansion in the *ab* plane ((220) peak at ~2θ ~36.5 °)

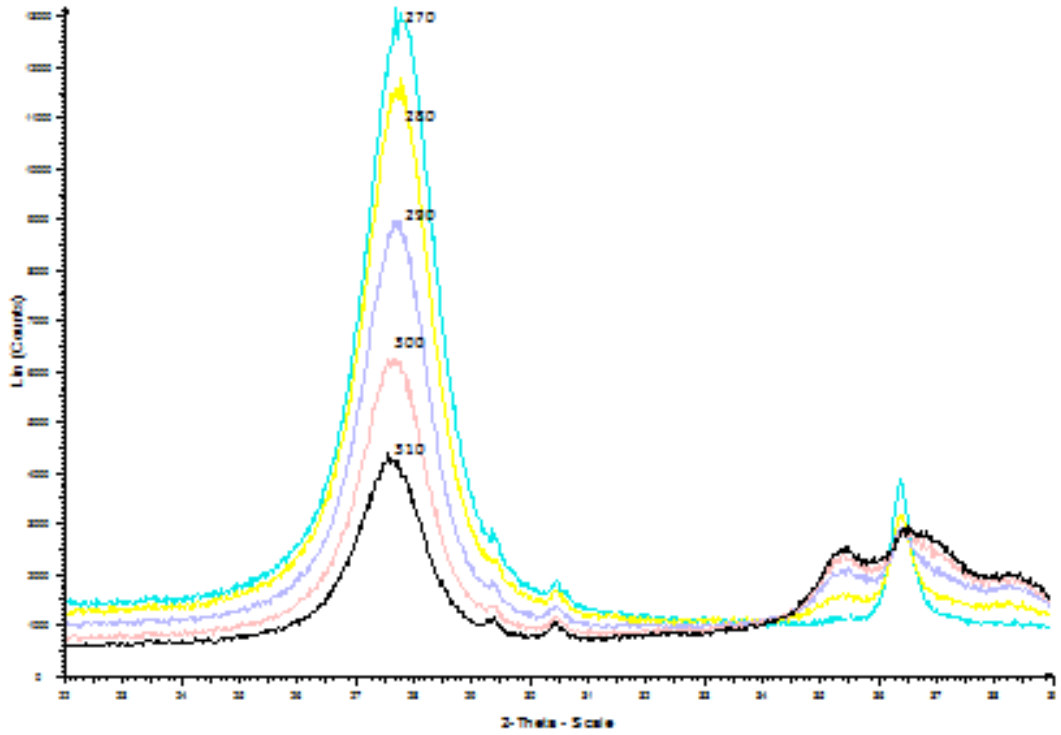

Figure S.13: X-ray diffraction patterns of $CuNi(CN)_4$ over the temperature range 270-310 °C (543-583 K) showing decomposition of the sample.

Table S.4: Linear thermal expansion coefficients for lattice parameters *a* and *c* and unit-cell volume, *V*, for $Ni(CN)_2$ and $CuNi(CN)_4$ measured using powder X-ray diffraction.

	α_a / 10^{-6} K^{-1}	α_c / 10^{-6} K^{-1}	α_V / 10^{-6} K^{-1}	T_{range} / K	Ref.
$CuNi(CN)_4$	–9.7 (8)	89 (9)	70(1)	93 – 543	
$Ni(CN)_2$	–6.5 (1)	68.8 (3)	48.5(5)	12 – 295	[1]
graphene layer	–8.0 (7)			200 – 400	[16]

4. Intercalation of 4,4'-bipyridine into $CuNi(CN)_4$

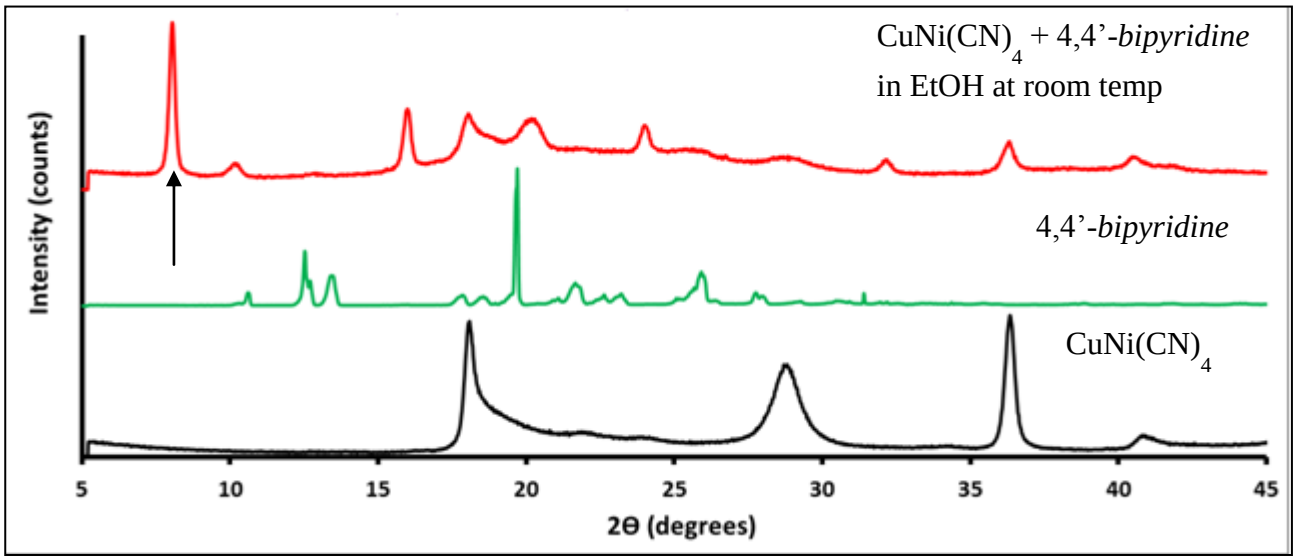

Figure S.14: Powder X-ray diffraction pattern of $CuNi(CN)_4$ after stirring in a solution of 4,4'-bipyridine in ethanol at room temperature for 1 week. Some $CuNi(CN)_4$ still remains in the final product but the appearance of a peak at ~11.3 Å corresponds to an increase in the interlayer separation consistent with intercalation of 4,4'-bipyridine between the $CuNi(CN)_4$ layers.

5. Exploring the Cu(II)-Ni(II)-CN Phase Diagram

5.1 Synthesis of Mixed Copper(II)-Nickel(II) Cyanide Hydrates, $Cu_xNi_{1-x}(CN)_2 \cdot 3H_2O$

Cu(II)-Ni(II) cyanide hydrates, $Cu_xNi_{1-x}(CN)_2 \cdot 3H_2O$ ($0 \leq x \leq 0.25$) were prepared from mixtures of metal chlorides with Cu:Ni ratios of less than 1:3 (Table S.5).

Aqueous solutions of $CuCl_2 \cdot 2H_2O$ and $NiCl_2 \cdot 6H_2O$ were prepared in separate flasks. These were quickly and simultaneously added to an aqueous solution of KCN. In each case, a green gelatinous precipitate immediately formed. The products were stirred for 10 hours, then filtered, washed with distilled water and allowed to dry in air. The resulting fine green powders were characterized using atomic absorption spectroscopy (Table S.5), IR and Raman spectroscopy (Table S.6) and powder XRD (Figure S.15, Table S.7). The powder X-ray diffraction patterns closely resemble that previously measured for $Ni(CN)_2 \cdot 3H_2O$.[17] TGA analysis further confirmed the compositions as $Cu_xNi_{1-x}(CN)_2 \cdot 3H_2O$. Similar reactions using reagents with Cu:Ni ratios between 1:1 and 1:3 produced a mixture of $CuNi(CN)_4$ ($Cu_{0.5}Ni_{0.5}(CN)_2$) and $Cu_{0.25}Ni_{0.75}(CN)_2 \cdot 3H_2O$ ($CuNi_3(CN)_8 \cdot 12H_2O$). The powder XRD pattern of the product of the attempted synthesis of $Cu_{0.375}Ni_{0.625}(CN)_4 \cdot 3H_2O$ clearly shows a mixture of phases (Figure S.16).

Table S.5: Preparation of the mixed Cu(II)-Ni(II) cyanide hydrates, $Cu_xNi_{1-x}(CN)_2 \cdot 3H_2O$

Composition	$CuCl_2 \cdot 2H_2O$	$NiCl_2 \cdot 6H_2O$	KCN	Cu:Ni ratio of reagents	Cu:Ni ratio from AA†
$Cu_{0.05}Ni_{0.95}(CN)_2 \cdot 3H_2O$	0.0343 g (0.20 mmol) in 10 ml H_2O	0.9044 g (3.80 mmol) in 10 ml H_2O	0.5245 g (8.05 mmol) in 10 ml H_2O	0.05	0.05
$Cu_{0.125}Ni_{0.875}(CN)_2 \cdot 3H_2O$	0.0853 g (0.50 mmol) in 15 ml H_2O	0.8312 g (3.50 mmol) in 15 ml H_2O	0.5225 g (8.02 mmol) in 15 ml H_2O	0.14	0.11
$Cu_{0.165}Ni_{0.835}(CN)_2 \cdot 3H_2O$	0.1127 g (0.66 mmol) in 10 ml H_2O	0.7939 g (3.34 mmol) in 10 ml H_2O	0.5220 g (8.02 mmol) in 10 ml H_2O	0.20	0.16
$Cu_{0.25}Ni_{0.75}(CN)_2 \cdot 3H_2O$ ($CuNi_3(CN)_8 \cdot 12H_2O$)	1.1423 g (6.70 mmol) in 75 ml H_2O	4.7800 g (20.1 mmol) in 75 ml H_2O	3.4906 g (53.6 mmol) in 75 ml H_2O	0.33	0.31

† The Cu:Ni ratio in the $Cu_xNi_{1-x}(CN)_2.3H_2O$ phases was verified by atomic absorption spectroscopy. Samples (typically 7-10 mg) were dissolved in 10 ml water containing ~0.02 g of KCN. The solutions were then diluted with distilled water prior to AA analysis using a novAA 350 Analytic Jena spectrometer (with λ = 500 and 341.5 nm for copper and nickel detection, respectively). The estimated standard deviation on the measured values is 2%.

5.2 Infrared and Raman Spectra of $Cu_xNi_{1-x}(CN)_2 \cdot 3H_2O$

Table S.6: IR and Raman spectra of hydrates (frequencies in cm^{-1})

		ν(OH)	ν(C≡N)	δ(HOH)	Low frequency modes
$Cu_{0.05}Ni_{0.95}(CN)_2 \cdot 3H_2O$	IR	3611 (s), 3498 (w), 3257 (w, br)	2165 (vs), 2129 (vw)	1621 (s)	
	R		2185 (vs), 2174 (s)		502 (vw), 448 (vw), 334 (w), 332 (w), 262 (w), 140 (vw)
$Cu_{0.125}Ni_{0.875}(CN)_2 \cdot 3H_2O$	IR	3608 (s), 3495 (w), 3208 (w, br)	2165 (vs), 2125 (vw)	1617 (s)	
	R		2191 (vs), 2178 (s)		502 (vw), 449 (vw), 399 (vw), 332 (w), 266 (w)
$Cu_{0.165}Ni_{0.835}(CN)_2 \cdot 3H_2O$	IR	3611 (s), 3489 (vw), 3257 (w, br)	2165 (vs), 2127 (vw)	1621 (s)	
	R	3623(vvw)	2195 (vs), 2181 (s)		502 (w), 449 (w); 331 (w), 291 (w, sh), 268 (w), 134 (vw)
$Cu_{0.25}Ni_{0.75}(CN)_2 \cdot 3H_2O$ $(CuNi_3(CN)_8 \cdot 12H_2O)$	IR	3612 (w), 3242 (w, v br)	2166 (vs), 2130 (vw)	1616 (s)	
	R		2214 (s), 2194 (vs), 2178(s)		508 (vw), 330 (w, br), 263 (w)
$Ni(CN)_2 \cdot 3H_2O$	IR	3612(s), 3502 (w), 3263 (m, br)	2166(vs), 2125 (vw)	1634(m)	Ref [17]

5.3 Room-temperature Powder X-ray Diffraction Studies of $Cu_xNi_{1-x}(CN)_2 \cdot 3H_2O$

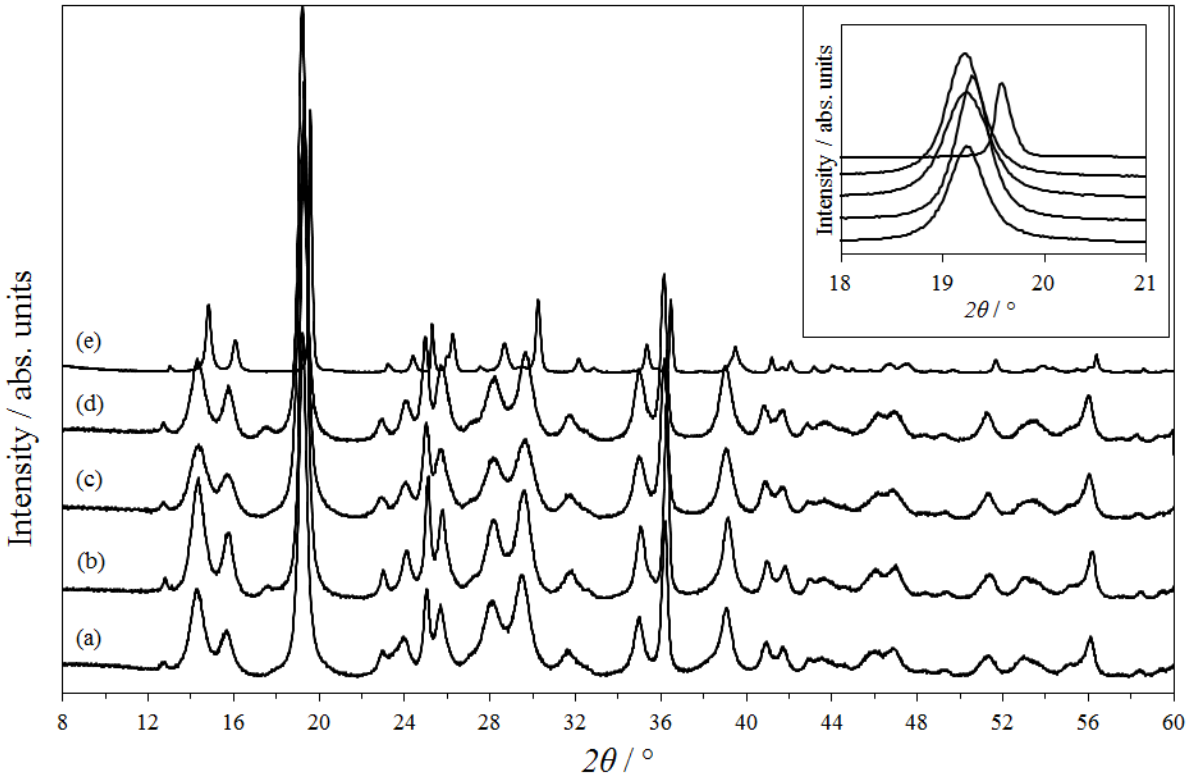

Figure S.15: Powder X-ray diffraction patterns at room temperature of $Cu_xNi_{1-x}(CN)_2 \cdot 3H_2O$: (a) $Cu_{0.25}Ni_{0.75}(CN)_2 \cdot 3H_2O$, (b) $Cu_{0.165}Ni_{0.835}(CN)_2 \cdot 3H_2O$, (c) $Cu_{0.125}Ni_{0.875}(CN)_2 \cdot 3H_2O$ (d) $Cu_{0.05}Ni_{0.95}(CN)_2 \cdot 3H_2O$ and (e) $Ni(CN)_2 \cdot 3H2O$.[17] In the inset, the 2θ region of 18–21 ° is enlarged for clarity.

Table S.7: Refined lattice parameters for $Cu_xNi_{1-x}(CN)_2.3H_2O$ at room temperature (space group *Pcmn*).

	a /Å	*b* /Å	*c* /Å	*V* /Å^3	Ref.
$Cu_{0.05}Ni_{0.95}(CN)_2 \cdot 3H_2O$	7.0459(9)	13.869(1)	12.366(1)	1208.4(2)	
$Cu_{0.125}Ni_{0.875}(CN)_2 \cdot 3H_2O$	7.051(1)	13.886(1)	12.361(1)	1210.4(8)	
$Cu_{0.165}Ni_{0.835}(CN)_2 \cdot 3H_2O$	7.0754(7)	13.860(2)	12.377(2)	1213.8(2)	
$Cu_{0.25}Ni_{0.75}(CN)_2 \cdot 3H_2O$ ($CuNi_3(CN)_8 \cdot 12H_2O$)	7.074(1)	13.874(2)	12.372(2)	1214.2(3)	
$Ni(CN)_2 \cdot 3H_2O$	7.1261(4)	13.8696(9)	12.2258(7)	1208.4(1)	[17]

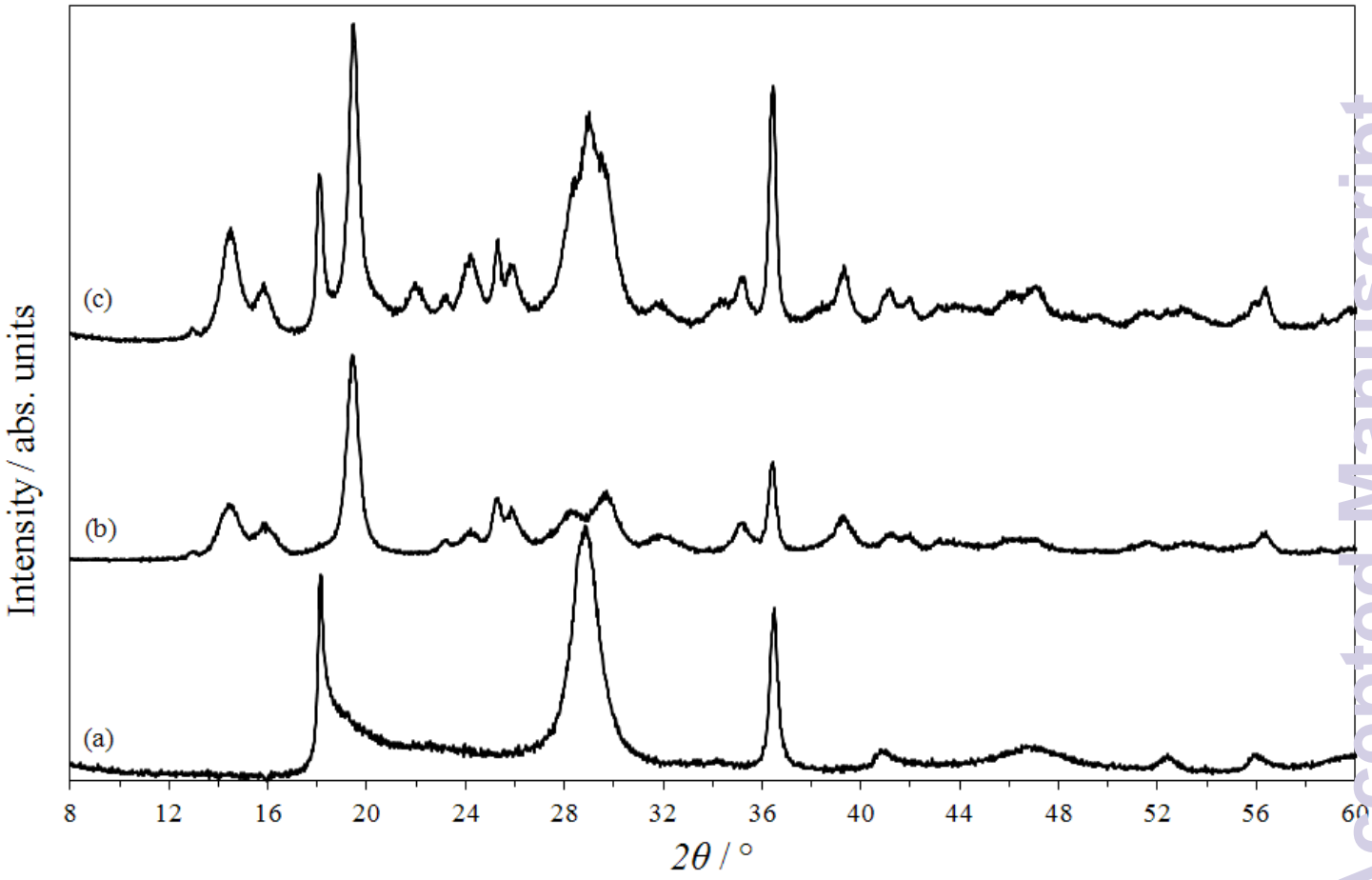

Figure S.16: Powder X-ray diffraction patterns at room temperature of (a) $CuNi(CN)_4$, (b) $Cu_{0.25}Ni_{0.75}(CN)_2 \cdot 3H_2O$ and (c) the product of the reaction of a mixture of $CuCl_2 \cdot 2H_2O$ and $NiCl_2 \cdot 6H_2O$ in KCN with a Cu:Ni ratio of 3:5. Product (c) is clearly a mixture of $CuNi(CN)_4$ and $Cu_{0.25}Ni_{0.75}(CN)_2 \cdot 3H_2O$.

5.4 Preparation and Characterisation of the Dehydrated Phases, $Cu_xNi_{1-x}(CN)_2$ ($0 \leq x \leq 0.25$)

The hydrated phases, $Cu_xNi_{1-x}(CN)_2 \cdot 3H_2O$ ($0 \leq x \leq 0.25$) were dehydrated by heating under vacuum at 400 K for 4 hours. The products were all red/brown in colour and rapidly rehydrated on exposure to moisture. The powder X-ray diffraction patterns were measured *in situ* at 403-413 K, as described in Section 3.2 page S18 (Figure S.17) and closely resemble those of $CuNi(CN)_4$ and $Ni(CN)_2$.

S26

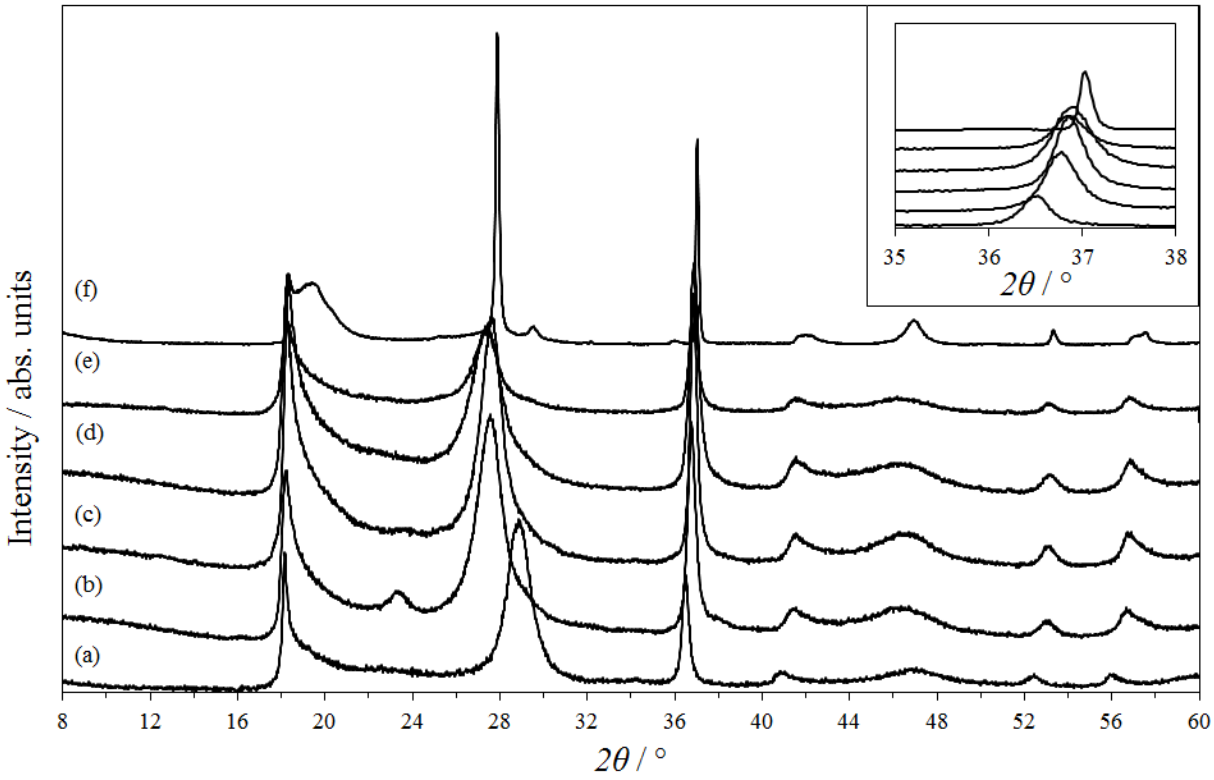

Figure S.17: The room-temperature powder X-ray patterns of (a) $CuNi(CN)_4$, (b) $Cu_{0.25}Ni_{0.75}(CN)_2$, (c) $Cu_{0.165}Ni_{0.835}(CN)_2$, (d) $Cu_{0.125}Ni_{0.875}(CN)_2$, (e) $Cu_{0.05}Ni_{0.95}(CN)_2$ and (f) $Ni(CN)_2$.[1]

5. References

(1) S. J. Hibble, A. M. Chippindale, A. H. Pohl and A. C. Hannon, *Angew. Chem. Int. Ed.*, 2007, **46**, 7116.

(2) S. J. Hibble, S. M. Cheyne, A. C. Hannon and S. G. Eversfield, *Inorg. Chem.*, 2002, **41**, 1042.

(3) F. Cataldo, *Europ. Polym. J.*, 1999, **35**, 571.

(4) G. D. Barrera, J. A. O. Bruno, T. H. K. Barron and N. L. Allan, *J. Phys.: Condens. Matter.*, 2005, **17**, R217.

(5) L. L. Bircumshaw, F. M. Tayler and D. H. Whiffren, *J. Chem. Soc.*, 1954, 931.

(6) P. Kubelka and F. Munk, Z. Tech. Phys., 1931, **12**, 593.

(7) A. C. Hannon in *Encyclopedia of Spectroscopy and Spectrometry* (*eds*. J. Lindon, G. Tranter, J. Holmes) Academic Press: London, 2000; Vol. 2; p 1479.

(8) A. C. Hannon, *Nucl. Instrum. Meth. A*, 2005, **551**, 88.

(9) A. K. Soper, A. C. Hannon, D. T. Bowron, S. E. McLain, *GUDRUN: a program for converting raw diffraction data to differential cross section*, 2006.

(10) A. C. Hannon, W. S. Howells, A. K. Soper, *Inst. Phys. Conf. Ser.*, 1990, **107**, 193.

(11) F. A. Akeroyd, R. L. Ashworth, S. L. Campbell, S. D. Johnston, C. M. Moreton-Smith, R. G. Sergeant, D. S. Silvia, *The ISIS Open Genie user manual*, Vers. 2.0, 1999, RAL-TR-1999-031, Rutherford Appleton Laboratory, Didcot, Chilton, UK

(12) E. Lorch, *J. Phys. C: Solid State Phys.*, 1969, **2**, 229.

(13) V. F. Sears, *Neutron News*, 1992, **3**, 26.

(14) S.J. Hibble, A.M. Chippindale, E. Marelli, S. Kroeker, V.K. Michaelis, B.J. Greer, P.M. Aguiar, E. Bilbé, E.R. Barney, and A.C. Hannon, *JACS*, 2013, **135**, 16478.

(15) S. J. Hibble, S. P. Cooper, S. Patat and A. C. Hannon, *Acta Cryst. B*, 1999, **55**, 683.

(16) D. Yoon, Y. W. Son and H. Cheong *Nano Lett.*, 2011, *11*, 3227.

(17) A. H. Pohl, *Solid-state architecture: from simple metal cyanides to open-framework materials*, Ph. D. Thesis, University of Reading, **2008**.

Graphical Abstract

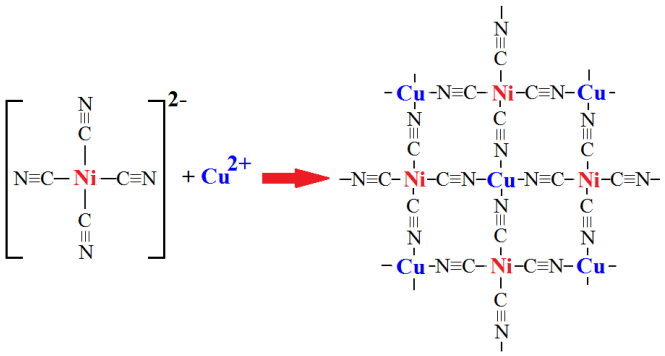

Cu(II) has been stabilised with square-planar coordination in a cyanide-only environment in the layered semiconducting material, copper-nickel cyanide, $CuNi(CN)_4$, which shows 2-D negative thermal expansion.